NNL Science

Issue 2 | February 2014

Feature Article

THE VITRIFICATION TEST RIG
A Research and Development Tool for High Level Waste Vitrification.

Also in this issue:

- **Molybdenum loading in glass**
- **Glass Leaching**
- **Hot Isostatic Press**
- **Strontium 90 mobility**
- **Corrosion in irradiated cooling water**

NATIONAL NUCLEAR LABORATORY

Scientific Journal

Contents

Introduction

Welcome to the second issue of "NNL Science".

We were delighted with the very positive feedback we received from readers of Issue 1 of NNL Science, published last summer. The resounding consensus was that it was an excellent vehicle for sharing some of the great scientific work we are doing across NNL's business, and a number of people commented that it was good to see a publication which went into detail across the range of different subject areas relevant to nuclear research.
I mentioned last time that one of the aims of the journal was to stimulate engagement between NNL and the wider scientific community, so we will continue to welcome any comments you may have - either to the article authors (whose contact details are provied at the start of each article) or to the editors.

In each issue we highlight one of NNL's key capabilities. This issue focuses on the vitrification test rig used to simulate the immobilisation of High Level Waste into glass.

Graham Fairhall *(Chief Science and Technology Officer)*

Editor's comments

It gives me great pleasure to introduce the second issue of the NNL Science journal. In this issue we take a look at established and new immobilisation technologies, the ability of glass materials to retain encapsulated elements, mobility of ^{90}Sr in contaminated groundwater and summarise an extensive body of work on the corrosion of steels in highly irradiated cooling water systems.

One of the cornerstones of a closed nuclear fuel cycle is the ability to demonstrate robust control of radioactive waste product materials and the current state-of-the-art for managing highly radioactive (self heating) waste is vitrification (immobilisation in a glass matrix). It is often difficult to convey the challenge of dealing with waste material that requires heavy biological shielding and remote operations i.e. using automation and mechanical arms. A great deal of thought and attention is required for even the simplest of tasks and so there is great benefit to having non-radioactive facilities that can reliably replicate active operational plants. The vitrification test rig (VTR) is a shining example of best practice in this area and has proven itself worthy of investment many times over by giving confidence in the quality of the waste products made over a range of operating envelopes. The articles here neatly demonstrate these benefits for both current operations and for future challenges. High molybdenum loading in glass is a timely example, where plant vessels will need to be cleaned free of high molybdenum containing radioactive solids prior to decommissioning.

Future decommissioning of nuclear sites also involves dealing with problem materials that do not fit into well established waste streams. This is another imminent challenge that NNL are at the forefront of, by developing a hot isostatic press in a nuclear environment to produce ceramic and glass-ceramic materials suitable for ultimate disposal. The technique is flexible and can be adapted to different feed materials from plutonium containing residues to ion exchange resins.

Decommissioning also requires dealing with contaminated land and assessing near field behaviour of the most potentially hazardous radioisotopes. In a fruitful collaboration with the University of Leeds we are providing a fundamental understanding of the mobility of radioisotopes such as ^{90}Sr in relevant environments helping to develop computer models and guide policy decisions.

Some policy decisions are problematic to judge, requiring high quality scientific evidence from situations that are difficult to replicate in the laboratory. One such example is water side corrosion in cooling systems that are subjected to very high radiation fields. Only by developing corrosion test samples that provide the stresses and strains of in-situ stainless steels, then applying the required radiation field and measuring the corrosion rates, can the suitability of corrosion inhibitors be assessed.

As always I would like to thank all of the authors for their contributions. I hope you find the articles interesting and any feedback you may have is always welcome.

Mark Sarsfield *(Editor, NNL Research Fellow)*
mark.sarsfield@nnl.co.uk

Katie Bell *(Assistant Editor)*
katie.j.bell@nnl.co.uk

THE VITRIFICATION TEST RIG – A RESEARCH AND DEVELOPMENT TOOL FOR HIGH LEVEL WASTE VITRIFICATION.

Nick Gribble and Rick Short
nick.r.gribble@nnl.co.uk

INTRODUCTION

The reprocessing of spent nuclear fuel involves the separation of uranium and plutonium from highly radioactive fission products that are heat generating and classed as High Level Waste (HLW). During reprocessing operations the waste is generated as a nitric acid solution containing many radioactive elements requiring remote handling. It became clear in the early days of fuel reprocessing that the HLW would need immobilising in a solid matrix to ensure safe handling and storage in the medium term. Dating back to the 1950s, vitrification technology was developed and eventually implemented on an industrial scale to immobilise the HLW in to glass in the UK at Sellafield and in France at La Hague

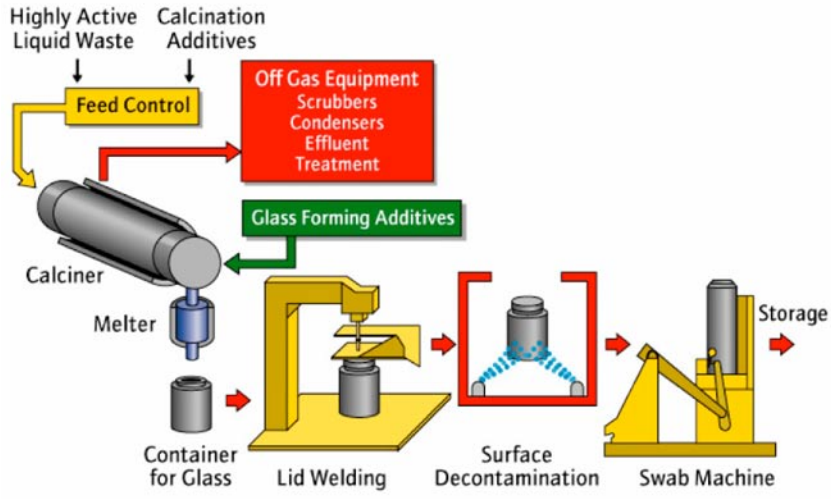

Figure 1: General overview of the processes on a waste vitrification line

The Waste Vitrification Plant (WVP) at Sellafield comprises three production lines that convert Highly Active Liquor (HAL) into a stable glass product with the active isotopes chemically bonded into a borosilicate glass matrix. Lines 1, 2 and 3 began operation in 1990, 1991 and 2002 respectively. In order to improve vitrification production throughput plans were developed to initiate several improvement projects to deliver the step change in performance that was considered necessary to accelerate the HAL stock hazard reduction strategy. The VTR forms part of these plans. A general overview of the process is illustrated in Figure 1.

The vitrification process

HAL is blended as required in one of two storage tanks and lithium nitrate is added because early development work identified that feeding some of the lithium with the HAL feed reduced the dust generated in the calciner and reduced the formation of a crystalline spinel phase in the product. A sample is taken for analysis at this point and is used to determine the feed rate to the process. The HAL is fed to one of the WVP feed tanks in 7 to 10m^3 batches and homogeneity is maintained in the tanks by use of steam ejector operated pulse jets that lift a volume of the HAL within a small internal vessel and then let it fall back by gravity. HAL is fed to the calciner by a constant volume feeder (CVF), together with recycle liquor from the dust scrubber and a sugar solution.

The calciner (Figure 2) comprises a rotating tube, inclined at a small angle that is heated by 4 pairs of resistance furnaces. Zones 1 & 2 are larger and more powerful than zones 3 & 4. Within the tube there is a loose metal bar, known as the rabble bar, which stops build up of material on the inside wall of the tube and reduces the particle size sufficiently for the dry calcine to enter the melter through narrow slots at the lower end of the tube. Special end fittings connect the calciner to the liquid feed and off-gas system at the upper end and the glass feed and melter at the lower end.

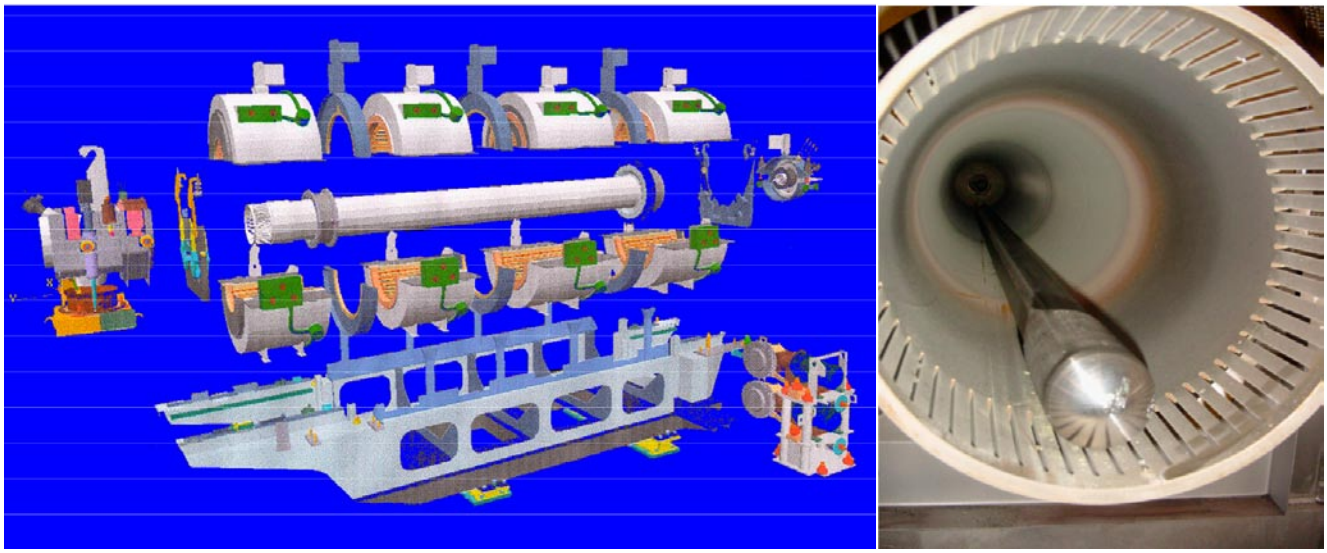

Figure 2: Exploded view of the WVP calciner & rabble bar inside the calciner tube

The liquid feed is directed onto the inner wall of the calciner tube and the evaporation process is completed at the end of the second heating zone. The solids produced are dried and partially denitrated in zones 3 & 4. The position of the evaporative front and the calcine properties are controlled by varying the temperature of the calciner heating zones and the rotational speed of the tube. The latter also impacts on rabble bar effectiveness and the rate of wear of the seals. Glass crizzle is fed into the calciner tube at the lower end and exits to the melter crucible with the calcine. The glass is fed in batches, usually at 3 minute intervals, weighing between 650 and 1200 g dependant on the glass production rate and the target waste oxide incorporation rate, i.e. the waste loading.

The WVP melter system is an induction heated elliptical metal crucible (Figure 3). In simple terms the alternating current in the coils within the inductors induce eddy currents within the melter crucible body and its resistance leads to Joule heating of the metal. Heat is transferred to the melt by conduction and radiation, so effective mixing is essential to ensure an acceptable reaction rate and good homogeneity at a relatively low differential temperature between the crucible wall and the melt, so as to minimise the corrosion rate of the crucible. Air or argon is fed to sparge pipes whose outlets are near to the base of the crucible to provide the agitation. The standard charge to the crucible for a feed cycle is 195 kg at a glass production rate of typically 20 to 25 kg/h and, assuming the melt is sufficiently hot, feeds are interrupted and the glass is poured by heating a freeze valve on the base of the crucible. A heel of about 70 kg of glass is maintained in the crucible after pouring, as the base of the crucible is not heated and this improves the overall production rate. Pouring typically takes 40 minutes to 1 hour. Two pours are made into each container, which is then allowed to cool to remove process heat prior to welding on the lid, after which the container is decontaminated by high pressure water jet and swabbed to check for external contamination. Once it meets the export requirements, the container is moved to the Vitrified Product Store (VPS), a passively ventilated store with a capacity for 8000 containers.

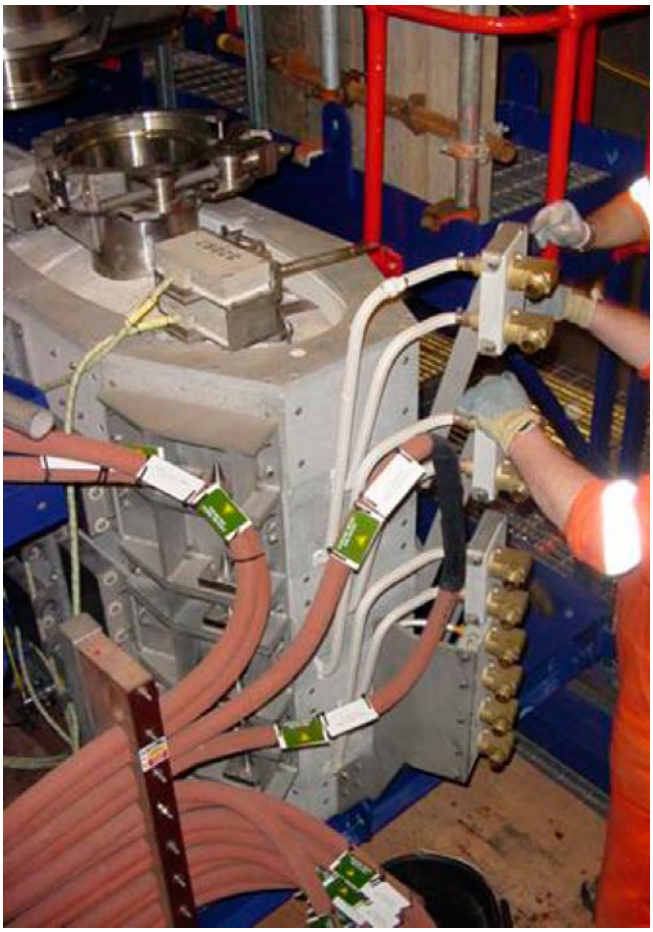

Figure 3: VTR melter crucible and induction stack

The off-gases from the calciner comprise of calcine dust, steam, nitric acid vapour, gases from decomposition of the feeds, inleakage of air at the calciner seals and the gas fed into the melter crucible and glass feed system. These pass into a dust scrubber (Figure 4) which removes about 95 % of the dust. The dust scrubber has 3 sections; the sump at the bottom, the torroidal centre section and the cascade in the top section. The off-gases enter tangentially into the central section which acts as a cyclone removing larger particles. The sump holds about 60 L of boiling nitric acid containing dissolved calcine which is airlifted to the top of the plated upper section of the column to form a cascade. The gases pass up through the inclined plates, counter current to the cascading acid, providing more dust removal by directional change and direct contact with the scrub liquor. When WVP is in HAL feed some of this liquor is fed back to the calciner to maintain a relatively low level of total solids in the liquor.

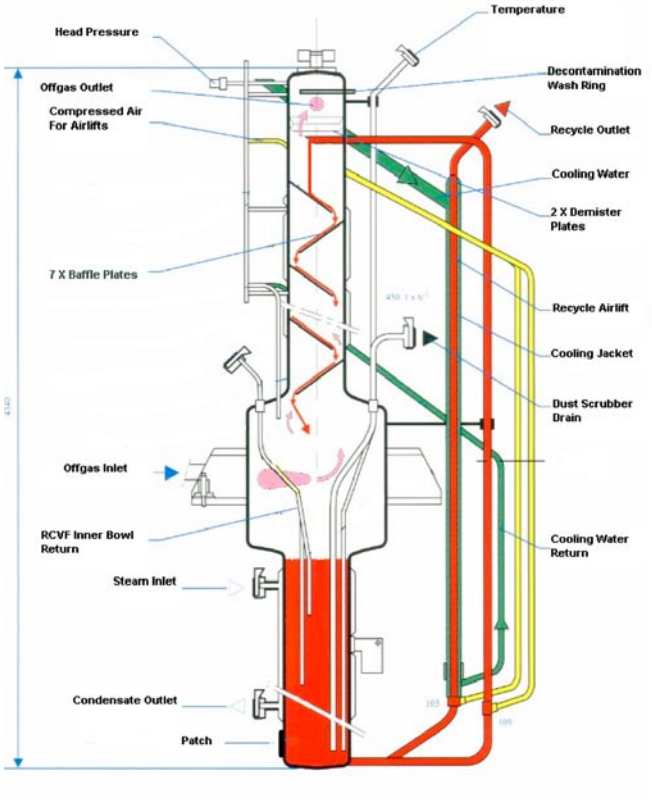

Figure 4: Schematic of the dust scrubber

After passing through 2 demister plates the cleaned gases and vapours exit the dust scrubber and are fed into the condenser, a 3 pass shell and tube heat exchanger, which removes the steam, nitric acid, most of the remaining dust and a significant amount of the NOx. The condensate is directed to the HA effluent tank and routed back to the HA evaporator. The off-gas proceeds to the NOx absorber, a bubble cap tray column, where most of the remaining NOx is removed. The low level of dust in the gases allow the use of this type of column without blockage of the trays. An air ejector maintains the melter, calciner and primary off-gas system at a small depression relative to the cell. Pressure control is maintained at the top of the dust scrubber at –15 mbar.

From 1996 the forerunner of NNL (i.e. the R&D department of British Nuclear Fuels Limited, BNFL) championed the construction of a full scale replica vitrification facility to provide the test bench upon which significant production improvements could be made and product quality underpinned. WVP cannot routinely sample its products and product quality is assured by operating the plant within a defined envelope that has previously been shown to make good quality glass. Making significant changes to the operational set points, waste incorporation rate or throughput at WVP requires evidence that the resulting product will be of acceptable quality. To generate that evidence, the Vitrification Test Rig (VTR) was sanctioned (2001), designed, constructed and commissioned, and began operation in 2004.

The business case for construction of the VTR was based on three premises; the potential to increase the waste oxide incorporation rate, increase the glass production rate and improve the plant availability. Additional benefits were perceived to be an improved understanding of the vitrification process and its limitations, the development of flowsheets for future waste compositions, the expansion of the existing WVP operational envelope, operator training, maintenance rehearsal, problem investigation and testing of new operational procedures. Its construction and continued operation represents significant research and development investment and demonstrates the commitment of firstly BNFL, then British Nuclear Group (BNG) and now Sellafield Ltd to reducing HAL stock levels and maintaining expertise in support of operational plant.

The chemical process

When HAL is processed it contains a certain amount of fission product elements (mainly metals) per tonne of uranium reprocessed. The amount depends on the burn-up of the fuel, cooling time and fuel type (uranium metal or uranium oxide) and associated non-active process additives from cladding/criticality control. The metals undergo two main chemical transformations as they pass through the vitrification process; calcination and vitrification:

Calcination

$$HNO_{3\,(aq)} + H_2O_{\,(aq)} + M(NO_3)_{y\,(aq)} \xrightarrow{\text{Heat}} MO_{z\,(s)} + NOx_{\,(g)} + H_2O_{(g)}$$

$$HNO_{3\,(aq)} + H_2O_{\,(aq)} + MO_y^{-x}{}_{\,(aq)} \xrightarrow{\text{Heat}} MO_{z\,(s)} + NOx_{\,(g)} + H_2O_{(g)}$$

Vitrification

$$\text{Borosilicate glass} + MO_{z\,(s)} \xrightarrow{\sim 1050°C} \text{Vitrified HLW}$$

The VTR is a full scale replica of the WVP feed, calcination and vitrification processes (Figure 5). It also reproduces the primary off-gas system (dust scrubber, condenser and NOx absorber) and has additional instrumentation and sampling capabilities. The feed to the plant is a non-radioactive simulant representative of the HAL processed in WVP, i.e. a nitric acid solution containing fission products and small amounts of fuel cladding and storage tank corrosion products.

The VTR can be operated in two basic modes; calcination and vitrification. Calcination trials are usually performed in advance of vitrification trials for significant changes in flowsheet or operating conditions. They require the removal of the melter and installation of a calcine collection system in its place that facilitates the regular sampling of the calcine made under a variety of conditions. Within the calciner the HAL simulant together with recycled dust scrubber liquor and a sugar (sucrose) solution are firstly evaporated, dried and then partially denitrated. The sugar solution is used to produce a less oxidising atmosphere that helps minimise ruthenium volatility, thereby reducing the challenge to the off-gas system. The calcine product, looking somewhat like instant coffee granules, is normally fed into the melter with the borosilicate base glass crizzle (0.5 to 2 mm particles). Calcination trials allow optimisation of the temperature and rotational speed of the calciner, definition of an acceptable temperature envelope in terms of calcine residual nitrate and hence reactivity of the calcine in the melter, and assessment of the effect of liquor and/or waste oxide throughput on the calcine product and the performance of the off-gas system. Once optimised calcination conditions are defined, vitrification trials can proceed and these may also include the extremes of the acceptable calcination operational envelope to allow qualification of products made under a wide range of conditions.

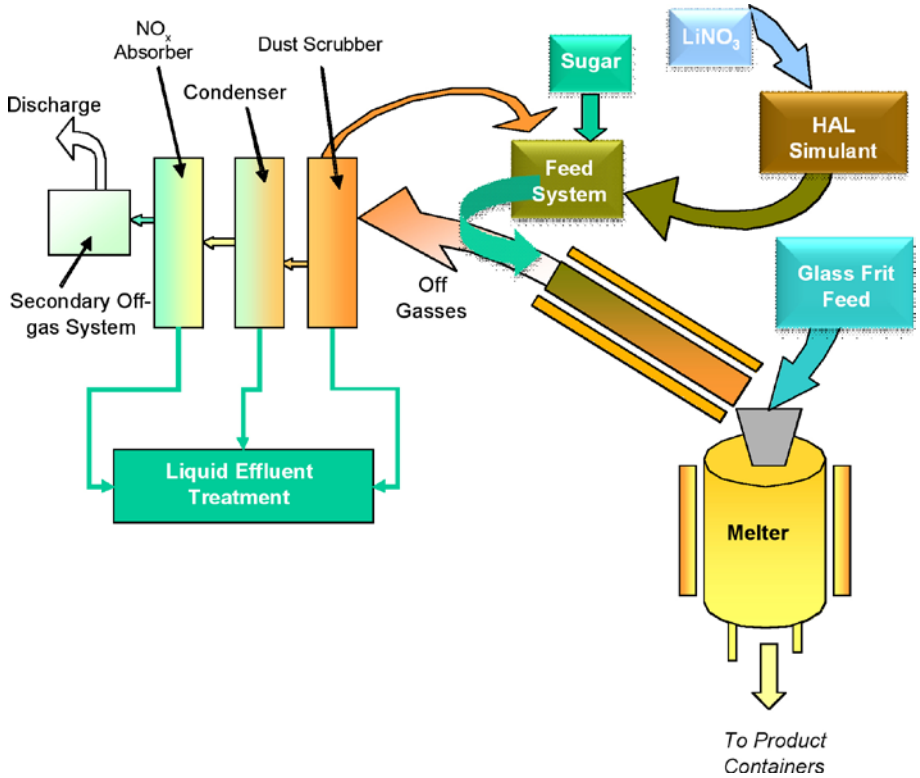

Figure 5: Schematic of the Vitrification Test Rig (VTR) operations

A range of waste types can be processed depending on the customer's requirements and the major objective is usually to ensure that any changes to the operating envelope still provides a suitable glass product. Vitrification trials for each waste type usually assess the impact of a range of waste oxide incorporation rates, glass production rates and operating conditions (e.g. melter temperature and air sparge mixing set points) to enable definition of the vitrification operating envelope. Additionally they may include alternative methods of feeding, an increase in the concentration of key elements, the study of fault conditions and long term operability at steady state to assess its impact on the primary off-gas system.

Incorporation rate

The incorporation is defined as the %w/w (or wt%) of waste oxides in the final glass product. On WVP, errors associated with sampling, analysis and feed systems are calculated in the worst case to result in an additional 3 wt% on the target incorporation rate of the final product. Hence, it is standard practice on VTR to manufacture products at waste oxide incorporations of WVP target +3 wt%, as well as the WVP target, to underpin product quality of all potential WVP products.

The initial experimental programme was developed in advance of the construction of the VTR as support for the business case. At the time of handover WVP was operating at a glass production rate of 19 to 21 kg/h with an incorporation rate of 25 wt% waste oxides. The first two VTR campaigns assessed the operation of the VTR under the same conditions as WVP and compared all equivalent operational parameters so as to ensure that the VTR was fully representative of WVP. This benchmarking exercise was essential to engender confidence at WVP for the implementation of changes to incorporation rate and throughput. The opportunity was also taken in these first campaigns to increase the production rate of the VTR to the basis of design value of 25 kg/h, to assess the impact on the products and the operation of the equipment.

The early work (Campaign 2) confirmed the VTR to be fully representative of WVP and demonstrated the opportunity to increase the throughput to 25 kg/h without detriment to either the products or the operability of the off-gas system. A phased implementation on WVP of some of the results of Campaign 2 occurred in 2006.

Oxide and Magnox wastes

Oxide wastes are the HLW fission products from reprocessing ceramic uranium oxide fuel within the THermal Oxide Reprocessing Plant (THORP), while Magnox wastes come from the reprocessing of uranium metal fuel from the Magnox reactors. With the higher burn-up (amount of fissile material used) of oxide fuel there is more fission product mass generated per tonne of fuel. Since starting vitrification operations in 1990 and up to approximately 1996, all the waste vitrified was HAL resulting from Magnox reprocessing. From July 1997 to date the majority of waste vitrified includes HAL arising from THORP which is blended with HAL from Magnox reprocessing. The blended waste typically contains 75wt% waste from Oxide reprocessing (THORP) and 25wt% waste from Magnox reprocessing but blends of 50 % Oxide : 50 % Magnox and 25 % Oxide : 75 % Magnox have also been vitrified and found to give acceptable glass durability (Figure 6).

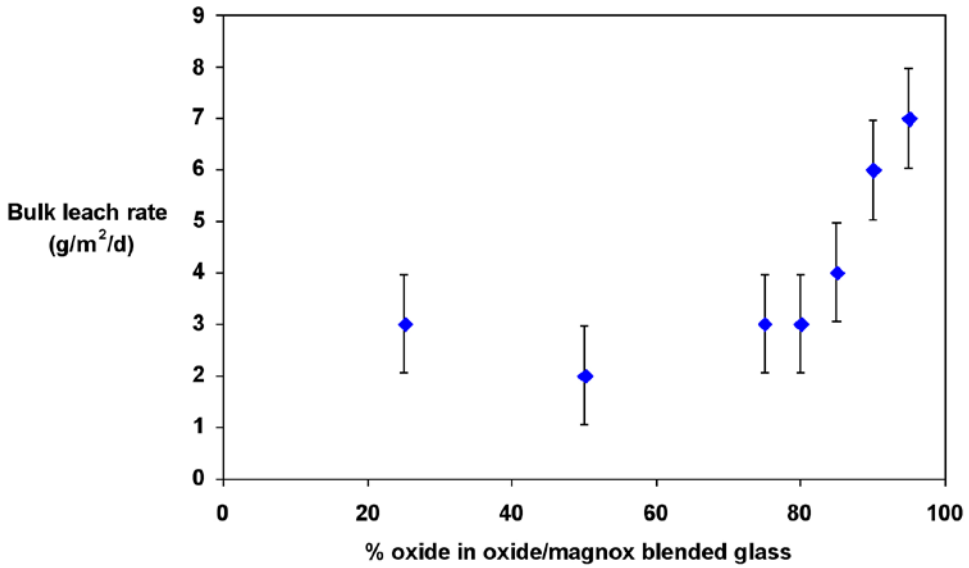

Figure 6: Bulk leach rate of various mixtures of Magnox and oxide blends

Campaign 3 raised the incorporation rate of blended Oxide and Magnox waste to 28 wt%. This was a very important improvement regarding the manufacture of products for overseas customers, as it maximised the waste loading in the products, from which the total fission product content is derived. Thus, the customers receive a smaller number of highly active containers for a given volume of waste, therefore delivering a business benefit directly to the customer by minimising their transportation, storage and final disposal costs. To ensure efficient transfer of research learning from VTR to WVP the key operational parameter changes were summarised in an implementation document with a stepwise transition from current to target conditions. Additionally, NNL personnel were seconded to WVP to brief the plant operators in advance of the change and to monitor the plant during the implementation, thus ensuring a smooth and confident transfer of knowledge and experience.

Campaign 4 introduced the use of the WVP designed multi-sparged melter crucible. The enhanced mixing within the multi-sparge melter crucible provided the opportunity to increase the throughput of blended Oxide:Magnox waste to 28 kg/h at 28 wt% incorporation. Campaign 4 also investigated the optimisation of the sugar feed rate and the effects of waste acidity and metal nitrate content. Sugar is added to reduce the loss of volatile ruthenium tetroxide by providing a reducing atmosphere in the calciner.

Figure 7 shows how the loss of ruthenium to the dust scrubber reduces as the level of sugar increases with respect to the amount of waste oxide fed to the process. However, at a high sugar feed rate the calcine becomes very dusty and dust losses to the off-gas system increase and can result in blockage of the calciner outlet and the dust scrubber recycle system and so an optimum of around 200-300 g sugar per kg of waste oxide is ideal. Later results showed that the ratio of the sugar to total nitrate content within the waste oxide was the key parameter to control and that there was a relatively broad acceptable range for sugar to total nitrate, with the optimum being 4.5 to 4.9 g_{sugar} /$mol_{total\ nitrate}$.

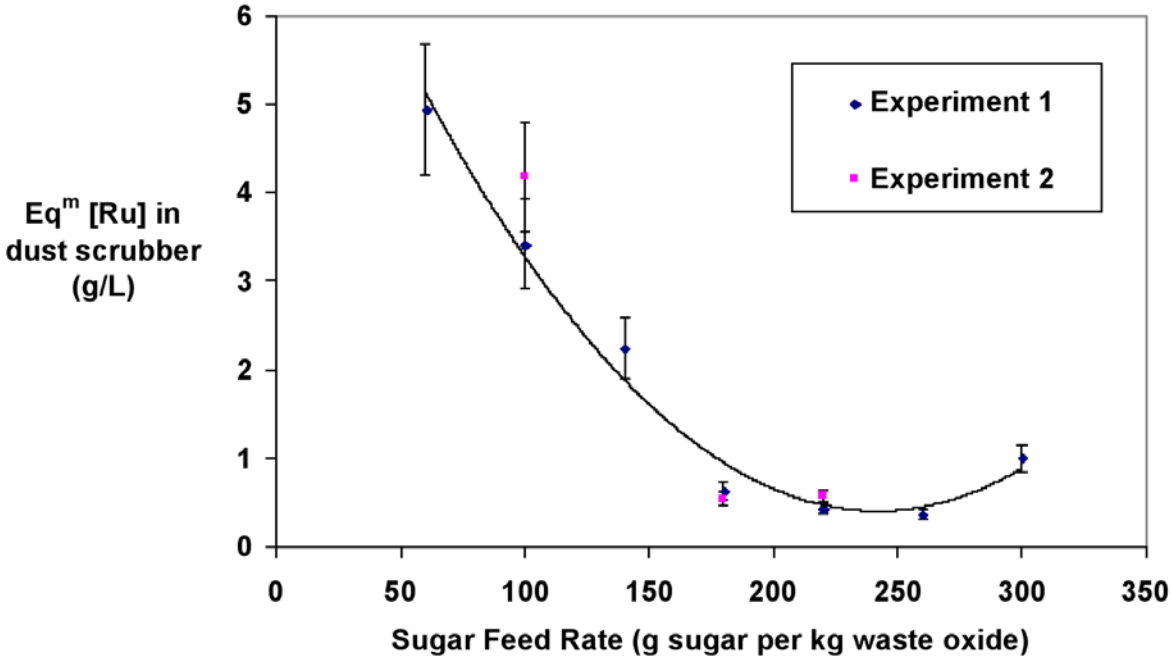

Figure 7: Dust Scrubber Liquor Ruthenium Concentration vs Sugar Feed Rate

These first campaigns provided the opportunity for WVP to significantly improve the HAL feed rate without compromising the product quality parameters for Overseas customers. For UK retained waste, opportunities existed to drive the waste loading much higher and as a result later VTR campaigns assessed Magnox and a range of Oxide:Magnox blend ratios at up to 38 wt% incorporation, so as to underpin product quality for WVP to operate up to 35 wt%. The main benefit of increasing the incorporation rate is that the number of product containers is reduced. The total cost of raw materials, production, packaging, storage and geological disposal is estimated to be several hundreds of thousands of pounds per container, so very significant savings can be made by increasing the incorporation rate. Savings made so far have been sufficient to recover more than the capital and operating costs of the VTR.

To achieve higher waste oxide incorporation rates without reducing the plant throughput required operation of the calciner both at significantly higher waste oxide and liquor throughput. To compound this problem, the concentration of waste oxides in the HAL feed is generally becoming more dilute due to shorter in-tank evaporation periods, thus requiring further increases in HAL feed rates to maintain target waste oxide throughputs. The Total Evaporative Load (TEL) fed to the WVP calciner prior to the VTR was invariably less than 57 L/hr, which comprised of the HAL, off gas recycle and sugar solution flows. To maintain the required waste oxide throughput at WVP it has been calculated that in the future a HAL feed rate of 55 L/hr will be required (recycle and sugar feeds increase the TEL to 76 L/hr). VTR has developed robust procedures for operating at 85 to 90 L/hr TEL at maximum HAL feed rate (69 L/hr), and trials have even demonstrated operation at 110 L/hr to be possible if the evaporative front is moved down the tube to the lowest acceptable position.

Table 1 summarises the throughput and incorporation rate increases achieved on the VTR and implemented so far on WVP.

containers and allowed the plant to operate routinely at optimised operating conditions to maximise plant life.

One of the key aspects to guaranteeing product quality is thorough analysis and characterisation of the glass produced on the VTR. This is carried out by NNL's team of highly experienced glass technologists who compile a continuous record of glass properties to ensure that the high incorporation, high throughput or out of specification products are of equal or better quality than any glass that was produced on WVP up to the implementation of the full scale research programme. In addition, the team regularly undertake laboratory scale optimisation studies to direct VTR campaigns and develop new glass formulations for trial at full scale.
The VTR team commonly collaborate with academia to encourage the exchange of knowledge, promote a fundamental understanding of the HLW product and ensure that cutting edge analysis techniques that may be applicable to the vitrification process are not overlooked. The most prolific academic partner has been the Immobilisation Science Laboratory at the University of Sheffield, where

Table 1: Summary of VTR and WVP improvements compared to basis of design

	Throughput (kg/h)	Incorporation Rate (wt%)	Evaporative load (g/L)	Waste Oxide Production (g/h)
Design	25	25	60	6250
WVP Max *% increase*	25 -	33 *28*	68 *13*	7000 *12*
VTR Max *% increase*	35 *40*	38 *52*	110 *83*	12160 *95*

One of the most significant benefits realised by WVP as a result of work performed on the VTR has been the underpinning of product quality of containers for the plant performance optimisation, the broadening of those limits and removal of unnecessary constraints. The acceptable ranges within the Plant Process Specification were not the limit of product quality, but defined the extent of work performed at the time the specification was generated (circa 1991). The VTR has provided data to allow removal of the requirement to operate the container pre-heat furnace, divorced the use of the sugar feed from product quality, significantly increased the allowable calciner rotational speed and expansion and demonstrated that the homogeneity of the feed is maintained without pulse jet mixing, so long as the recirculation of HAL to the Constant Volume Feeder (CVF) is continued. These VTR tests have underpinned the quality of hundreds of WVP

NNL has supervised vitrification related Masters, PhD and Postdoctoral research projects since it's inception in 2000. These projects have covered the measurement and modelling of glass viscosity, the formation, development and mitigation of secondary phases, analysis of glass structure at the atomic scale through techniques such as TEM, EELS, XPS, XAS and EXAFS, and a wide range of chemical durability testing including a collaborative project with our Belgium partners SKC.CEN on the NF-PRO glass dissolution project. In addition, the VTR glass technology team has collaborated with the University of Cambridge, University of Manchester, and Savannah River National Laboratory in the USA to develop their understanding of their HLW product. Investment in academic research has also provided the additional benefit of being able to train, develop and recruit new scientists and engineers to come to work in the nuclear industry.

Current Work

The focus of the VTR work has shifted from plant improvements to future feeds and problem solving. The main areas of work are now associated with the reduction of WVP availability caused by the deposition of caesium pertechnetate ($CsTcO_4$) in the connection between the dust scrubber and the condenser in the near term. In the medium term, and once reprocessing comes to an end, there will be challenges for dealing with Post Operational Clean Out (POCO) waste residues of the highly active storage tanks (HASTs) from which the HAL feed is delivered.

Due to changes in the operating philosophy of some waste streams the level of technetium in the HAL is higher than it used to be and is increasing with time. Technetium is volatilised from the melt as $CsTcO_4$, particularly from the reacting calcine on the surface, but additionally from a salt phase that forms in the glass product once the (low) Tc solubility limit is exceeded. The current dust scrubber design is not efficient at removing the 2 to 3 micron particles of condensed $CsTcO_4$ and they agglomerate in the gas outlet of the dust scrubber and block the route to the condenser. Blockage removal is currently necessary after around 6 feed cycles and requires cessation of feeds to wash out the pipe work (see Figure 8).

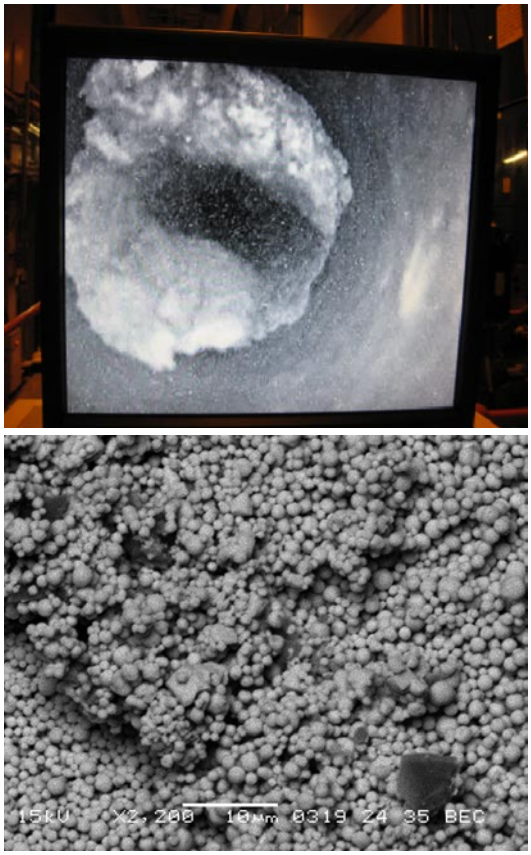

Figure 8: Endoscope image of the $CsTcO_4$ blockage in the WVP dust scrubber –condenser pipework (top) & backscattered SEM image of agglomerated $CsReO_4$ particles in the VTR pipework (bottom)

Using rhenium as a surrogate for technetium, VTR Campaign 13 investigated the effect of physical and chemical changes to the feed to the calciner, and changes to the operational parameters in the calciner, melter and dust scrubber to assess whether there was a way to reduce the volatility of $CsTcO_4$ or increase the capture efficiency of the dust scrubber. It was found that the inclusion of sodium in the HAL feed and the reduction of melter temperature and reheating prior to pouring had a positive effect, though the latter has the potential to increase stress within the melter crucible that could reduce its operational life. For VTR Campaign 14 a new dust scrubber with a glass upper section will be fitted into the VTR. A number of new designs in the upper plated section will be tested together with changes in certain operational parameters to try to improve its efficiency.

VTR Campaign 15 will concentrate on the vitrification of POCO wastes expected to be predominantly zirconium molybdate (ZM) and caesium phosphomolybdate (CPM) with an equivalent molybdenum oxide (MoO_3) content of about 60 % of the total metal oxides. MoO_3 has a relatively low solubility in borosilicate glass and an excess of MoO_3 results in phase separation of a partially water soluble yellow phase comprising alkali, alkaline earth and rare earth molybdates.

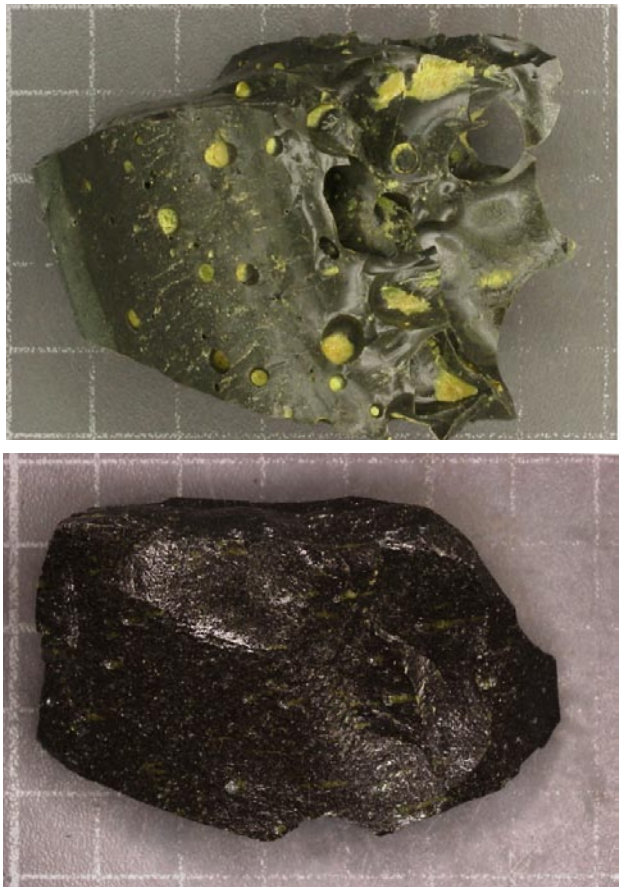

Figure 9: A simulated 38 wt% HLW incorporation glass with >10 wt% MoO_3 level showing the presence of yellow phase in the standard base glass frit (top) and the absence in the modified base glass composition (bottom). Scale markers = 1 cm^2

To solve this problem, extensive laboratory trials have resulted in the development of a new glass formulation that can be used at the existing melter operating temperature to incorporate vastly increased levels of MoO_3. Trials on the VTR using a basic chemical simulant have shown that phase separation would be expected to occur at around 5.3 wt% MoO_3 at 38 wt% total waste oxides with the current base glass formulation. Phase separation was not present even at 11.4 wt% MoO_3 in the improved base glass. The durability of the glass was as good as a standard product and there was no preferential leaching of Mo. Future work on the VTR in Campaign 15 will use a suitable physiochemical simulant, i.e. containing ZM and CPM, to study the calcination process and the effect of processing POCO solids on the losses to, and operation of, the primary off-gas system. Molybdenum is known to have the potential to form sticky solids that could block up the calciner, so calcination trials using an accurate POCO simulant are essential in advance of feeding POCO waste to WVP.

CONCLUSIONS

The VTR has demonstrated significant improvements in waste oxide incorporation rates compared to the WVP baseline flowsheet for all likely feed compositions and implementation of the results on WVP is progressing well. With more waste in every container the lifetime savings amount to several hundred containers each of which reduces total production, storage, packaging, transport and disposal costs by hundreds of thousands of pounds. There are no longer any WVP products without underpinning product quality data for the glass and the enhancement of the operating parameters in the Process Specification has maximised WVP availability and plant item longevity. A programme of work to support POCO of the HASTs and minimise the number of containers resulting from the recovery of the solids is progressing well and will result in very significant savings for Sellafield Ltd. The output from the VTR has fully justified its construction and operation and continues to receive strong support not only from high level waste plant management but also the Nuclear Decommissioning Authority and the Office of Nuclear Regulation who support Sellafield Limited to safely accelerate the HAL stock hazard reduction programme.

Acknowledgements

The Authors would like to thank Sellafield Ltd for sponsoring this work on behalf of the Nuclear Decommissioning Authority.

References

1. R. Short, N. Gribble, E. Turner, A. Riley, "Using the Vitrification Test Rig for Process Improvements on the Waste Vitrification Plants, "Advances in Science and Technology", **73**, 176, (2010).

2. S. Morgan, R.J. Hand, N.C. Hyatt, W.E. Lee. "Interactions of Simulated High Level Wastes (HLW) Calcine with Alakline Borosilicate Glass". MRS Proceedings, 807, 151 doi: 10.1557/PROC-807-151.

See also references in the following 2 articles.

A NEW GLASS FORMULATION FOR THE VITRIFICATION OF HIGH MOLYBDENUM WASTE

Barbara Dunnett, Nick Gribble and Rick Short
barbara.f.dunnett@nnl.co.uk

INTRODUCTION

In the UK, the Sellafield site Waste Vitrification Plant (WVP) currently immobilises highly radioactive liquors, produced from the reprocessing of spent nuclear fuel, into a borosilicate glass. Future challenges for WVP include the washout of solids from the base of the waste storage tanks in preparation for decommissioning, which will result in high molybdenum feeds. Molybdenum has a low solubility in the current alkali borosilicate frit used on WVP, however laboratory experimental work has led to the development of a new calcium borosilicate glass formulation that can incorporate up to 10 wt% molybdenum oxide (1).

Vitrification of a high molybdenum feed has been carried out, using non-active simulants, on the Vitrification Test Rig (VTR), which is a full scale working replica of a WVP processing line. This paper discusses the results of both the laboratory and full scale trials.

Background

At Sellafield site, highly active liquors produced from reprocessing of spent nuclear fuel are stored in a series of Highly Active Storage Tanks (HASTs) prior to being immobilised in a borosilicate glass. Post Operative Clean Out (POCO) of these tanks prior to decommissioning will involve the removal of caesium phosphomolybdate (CPM) and/or zirconium molybdate (ZM) solids. This will produce feeds to WVP enriched in molybdenum, which is known to have a low solubility in borosilicate glasses (2-4). Consequently, the vitrification of these solids in the current borosilicate glass formulation used on WVP is expected to be limited by the maximum %w/w molybdenum that can be incorporated, leading to a higher than desirable number of vitrified waste containers.

Glasses containing calcium, are able to trap the molybdenum as $CaMoO_4$ forming a stable durable phase in a vitreous medium (5, 6). Such glasses, which contain a significant quantity of crystalline inclusions, are known as glass composite materials (4-8).

Experimental

A series of borosilicate glasses containing 3.5 wt% Al_2O_3, 5 wt% CaO, 5 wt% ZnO and either 6, 8 or 10 wt% MoO_3 in the product were manufactured in the laboratory. BaO, Cs_2O, P_2O_5 and SrO were present in the glasses manufactured as these species are likely also to be present in the high molybdenum feed stream. A further borosilicate glass composition (VTR), which contained 8.67 wt% MoO_3, 3.68 wt% Al_2O_3, 4.95 wt% CaO and 2.20 wt% ZnO was manufactured both in the laboratory and on the VTR. ZrO_2 was also added as an additional species present in the high molybdenum feed stream. The compositions of the glasses are given in Table 1.

Table 1: Target composition of the borosilicate glasses

	6 wt% MoO_3	8 wt% MoO_3	10 wt% MoO_3	VTR
	Wt%			
Al_2O_3	3.5	3.5	3.5	3.68
BaO	1.84	1.84	1.84	1.83
CaO	5	5	5	4.95
Cs_2O	2.52	2.52	2.52	0.32
MoO_3	6	8	10	8.67
P_2O_5	0.41	0.41	0.41	0.05
SrO	0.14	0.14	0.14	0.14
ZnO	5	5	5	2.20
ZrO_2	-	-	-	3.16
B_2O_3	17.52	17.05	16.59	16.54
Li_2O	4.44	4.32	4.20	3.46
Na_2O	9.08	8.84	8.60	8.38
SiO_2	44.58	43.40	42.22	46.61

For the glasses manufactured in the laboratory, the required chemicals were weighed out and combined together using a rotary powder mixer. The powder to be melted was placed in a silica crucible and then into a furnace at 1050 °C for 4 hours. After 3 hours melting, the crucibles were removed from the furnace and stirred using a glass rod before being placed back into the furnace. The crucible was removed from the furnace after

a further hour at 1050 °C, and the glass poured into brass moulds to produce ingots that were then placed in an annealing furnace at 500 °C for 3 hours and then cooled to room temperature at a rate of 0.5 °C/min.

The resulting ingots were all subjected to optical examination. The ingots and the residues left in the crucibles were visually examined for phase separation, unincorporated material or any other features and photographed at low magnification.

The glasses were examined by a Scanning Electron Microscope (SEM) to give images of the vitrified product at the micron scale. Energy-Dispersive Spectroscopy (EDS) was carried out to determine the elements present within different areas of the glass. Finally, Raman spectroscopy and X-ray diffraction (XRD) was used to identify crystalline material present in a selection of the glasses.

Samples with the VTR composition were manufactured at the lab scale and also using the full scale Vitrification Test Rig (VTR) (9). Ca, Al, Zn and Li (equivalent to half of the Li_2O in the product) was added to a high molybdenum nitric acid feed stream containing Ba, Cs, P, Sr and Zr, which was then fed into a rotating kiln furnace known as a calciner to evaporate the liquor and de-nitrate the resulting solids to produce a calcined product. The calcine was mixed with a borosilicate glass frit (Si, B, Na and the remaining Li) in an inconel melter crucible and heated to ~1050 °C using an induction heating system. The melt was sparged with air to enhance mixing. The resulting melt of ~190 kg was then poured into a steel container, which after cooling, was split open and samples of the glass taken for analysis.

Results and Discussion

The laboratory glasses manufactured were all white in colour and no unincorporated phases were visually observed for the glasses containing ≤8.67 wt% MoO_3. The glass containing 10 wt% MoO_3 occasionally exhibited a number of brown spots, examples of which are shown in Figure 1. The size and quantity of this feature was variable between nominally identical samples. Raman spectroscopy was carried out on the white area (bulk material) and the brown spots. $CaMoO_4$ and $BaMoO_4$ were identified in both areas by the vibrational bands for the Mo-O stretches in the 750-1000 cm^{-1} region (Figure 2). The ratio of $BaMoO_4$ to $CaMoO_4$ appeared to be higher in the brown regions compared to the bulk material.

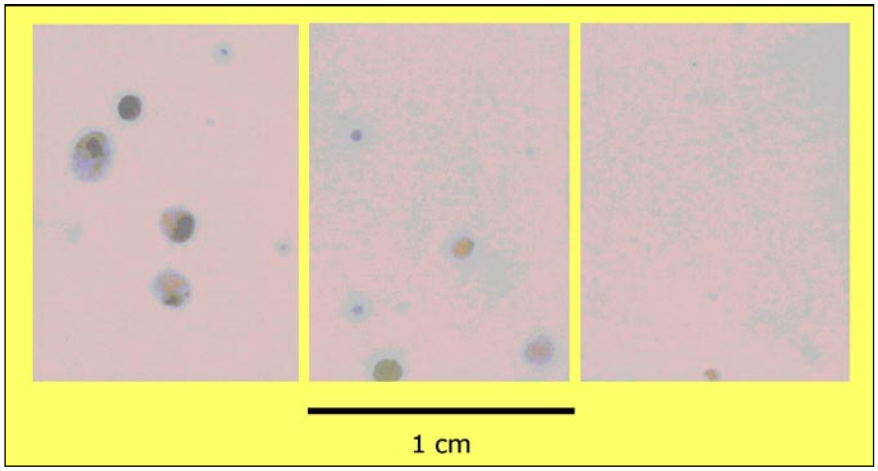

Figure 1: Brown spots occasionally observed on samples containing 10 wt% MoO_3

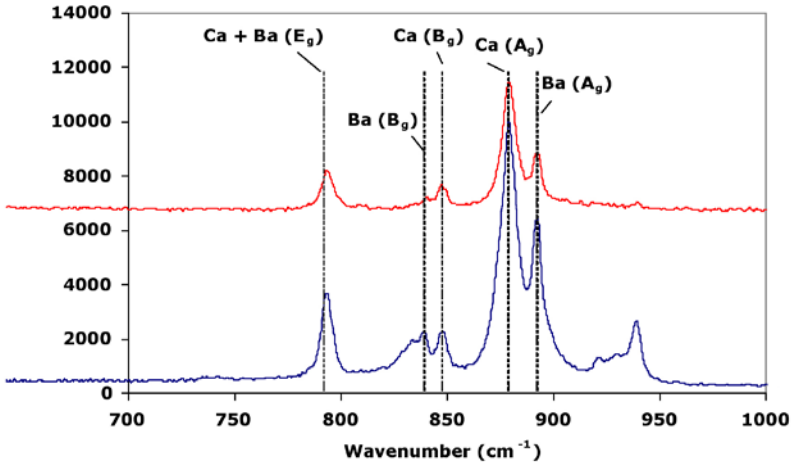

Figure 2: Raman spectra (top) of the white area (bulk material) shown by the red line and (bottom) the brown spots shown by the blue line

SEM examinations carried out on the borosilicate glasses containing 6, 8 and 10 wt% MoO_3 revealed the presence of a crystalline phase that had the appearance under SEM back-scattered electron mode (of white spots). The crystalline phases observed as a function of increasing MoO_3 are shown in Figure 3. EDS spotlight analysis of the crystalline spherical phase was carried out as indicated in Figure 3 and found that the phase was rich in calcium and molybdenum suggesting the presence of $CaMoO_4$, with some areas also being rich in barium suggesting the presence of $BaMoO_4$ or $Ca_xBa_yMoO_4$. The 6 wt% MoO_3 sample was submitted for XRD analysis which confirmed the presence of $CaMoO_4$. No matches for either $BaMoO_4$ or MoO_3 were identified in that sample.

Although the crystalline phase composition in all the glasses was similar, there was some variation of the size and distribution of the molybdate particles in the samples with increasing MoO_3. Figure 3 shows that in the glass containing 6 wt% MoO_3 the molybdate spheres are small and densely populated throughout the glass. Increasing the MoO_3 content to 8 wt% significantly increased the size of each molybdate particle scattered throughout the glass. Increasing the MoO_3 further to 10 wt% slightly increased the size of the individual particles and increased their population throughout the glass.

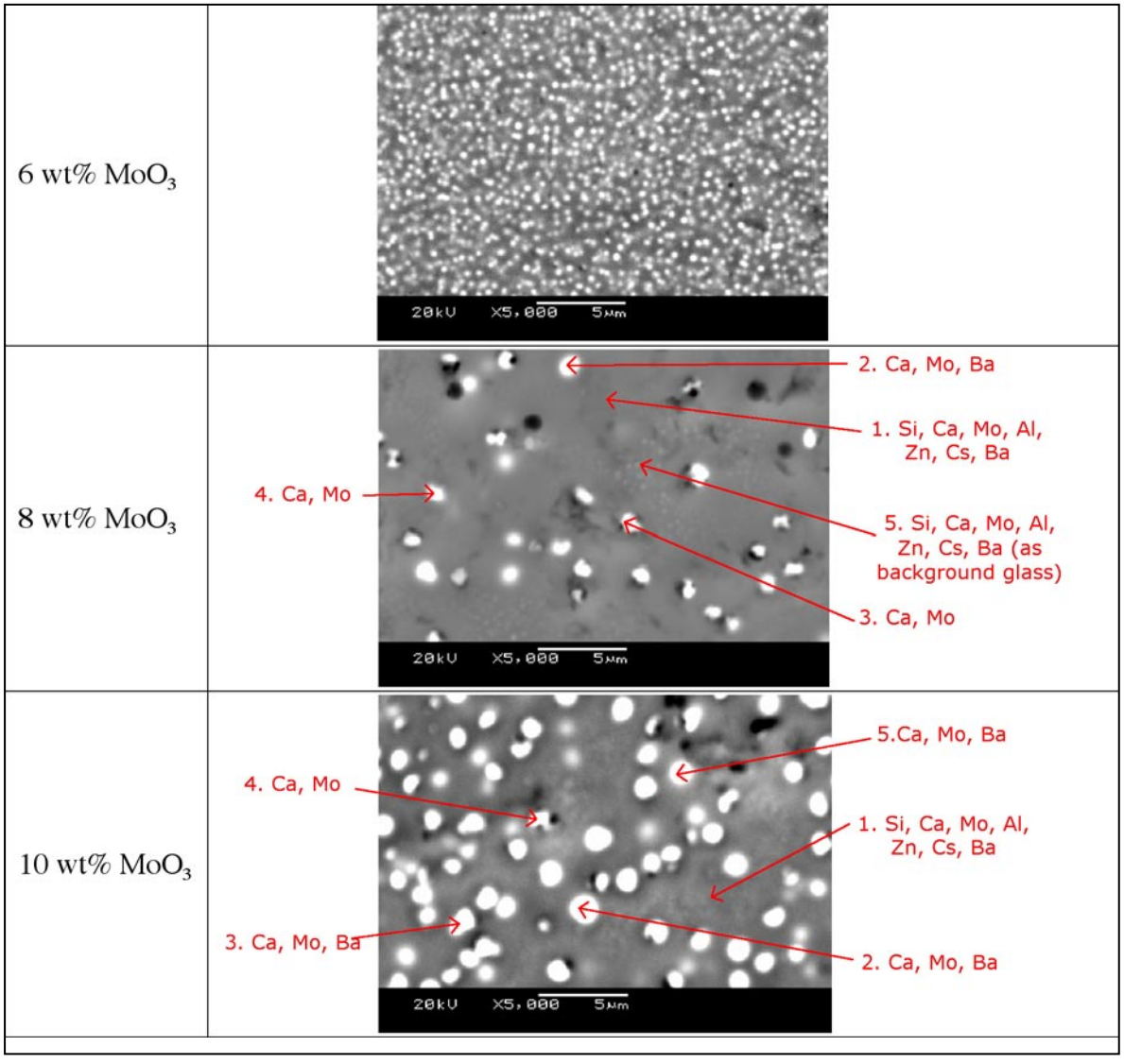

Figure 3: SEM analysis of product glasses containing 6, 8 or 10 wt% MoO_3

Spherical crystalline phases were also present in glass manufactured in the laboratory that contained ~8.7 wt% MoO_3 as shown in Figure 4. The formulation was successfully manufactured at a larger scale using the VTR without any process difficulties. The bulk leach rates were considered to be acceptable being comparable to those measured for WVP simulated product glass (1- 6 g/m^2/d). SEM examination of the product glass manufactured on the VTR revealed the presence of a crystalline spherical phase. In addition larger particles were observed as shown in Figure 5, which were analysed by EDS as being rich in calcium and molybdenum. Occasionally elongated particles were observed but only in selected areas of the glass. Where larger particles were observed, there were no smaller ones in their vicinity suggesting that these particles had formed by agglomeration of the smaller spherical particles. XRD analysis was carried out on both the glasses manufactured on the VTR and in the laboratory. The traces obtained were very similar with matches for both $CaMoO_4$ and $BaMoO_4$ (Figure 6). Hence the difference observed in the phase morphology was not due to the presence of different crystalline phases. In the laboratory, the glass melts (~30 g) are removed from the furnace, which is at 1050 °C, and poured into a mould to form an ingot. The ingot is then placed in a furnace at 500 °C to be annealed. Hence rapid cooling of the melt occurs. On VTR, the glass is poured into a cylindrical steel container with an internal diameter of 0.35 m preheated to 650 °C. This in conjunction with the larger mass of glass (~190 kg), originally at a temperature of ~1057 °C results in slow cooling of the melt; and only cooling to ~500 °C in ~10 hours. There will be some differences within the melt as the external surfaces cool at a greater rate than the centre of the pour. Hence, it is possible that some agglomeration of the spherical phase occurs as the glass cools during the time it is above the glass transition temperature, which although not measured for the calcium molybdate glasses, is typically between 505 and 535 °C for WVP borosilicate glasses. Additionally, some agglomeration of the spherical phase may have occurred during mixing of the glass melt whilst molten in the VTR melter. The laboratory glass was only stirred once during the four hour melt, whereas the glass in the VTR melter was continually mixed by air sparging.

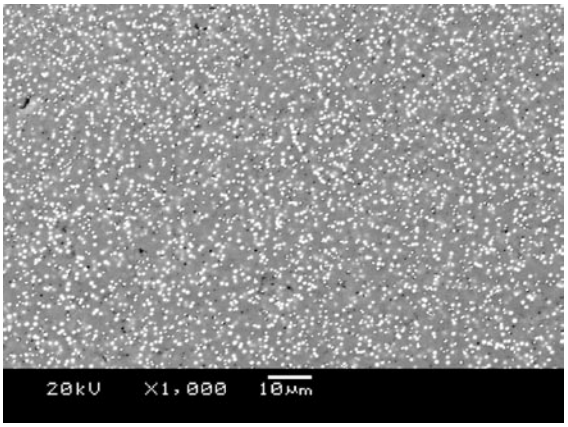

Figure 4: SEM photograph of VTR glass composition fabricated in the laboratory

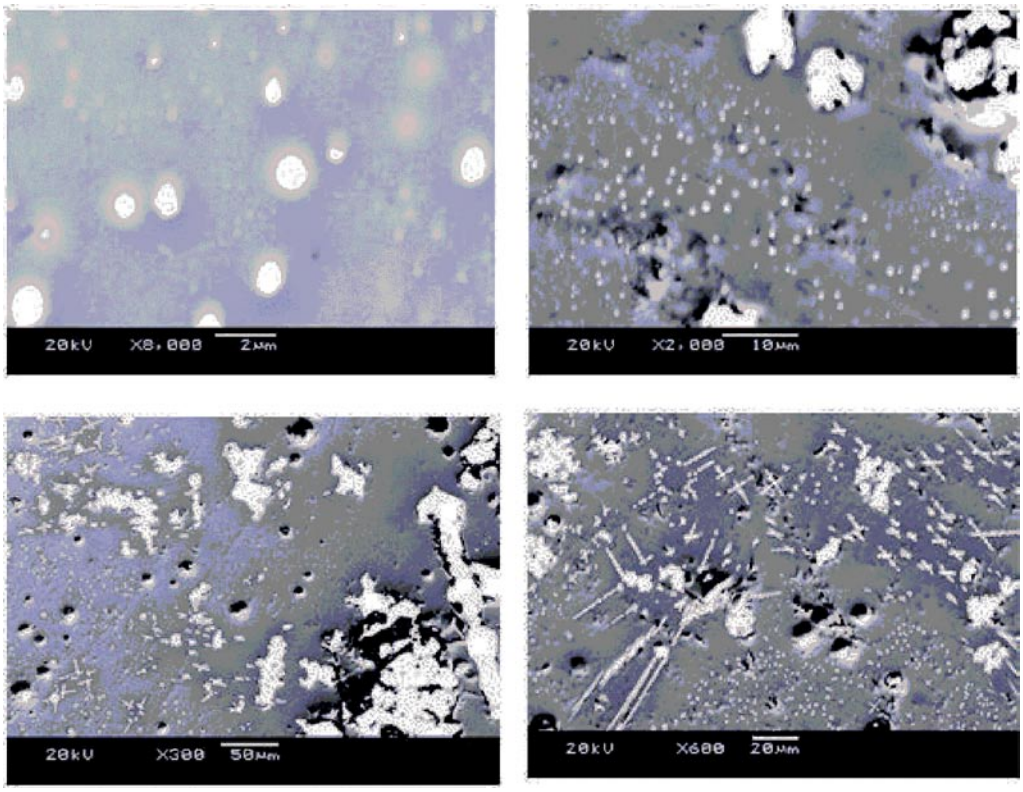

Figure 5: SEM images showing the morphology of molybdate particles observed in the glass manufactured on the VTR

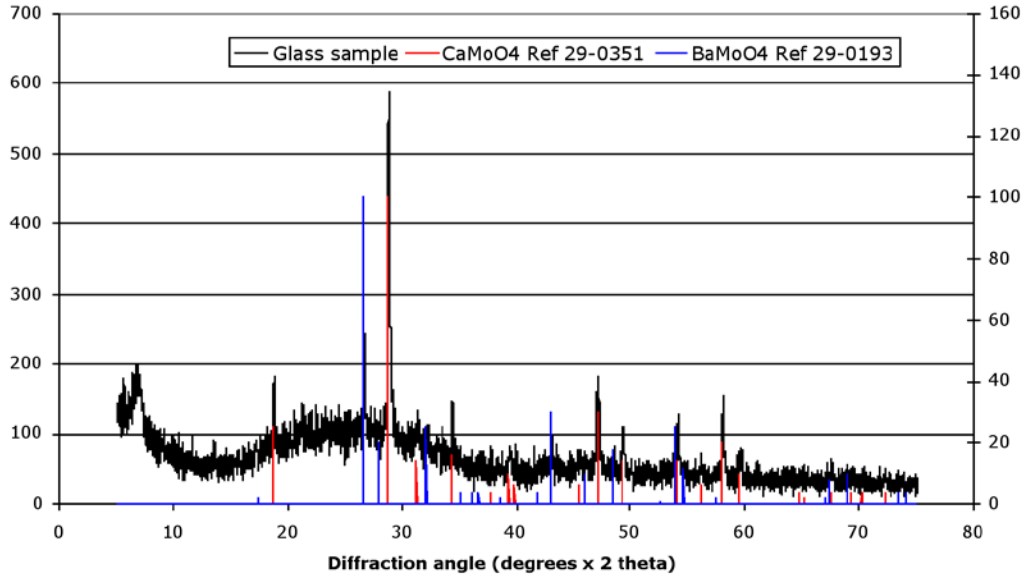

Figure 6: XRD pattern showing presence of $CaMoO_4$ and $BaMoO_4$

CONCLUSIONS

High molybdenum feeds can be vitrified with borosilicate glasses containing CaO, ZnO and Al_2O_3 at a melt temperature of ~1050 °C. In this study, glasses containing up to 10 wt% MoO_3, were successfully manufactured. The large quantity of MoO_3 was vitrified by trapping the molybdenum as a durable $CaMoO_4$ or $BaMoO_4$ phase.

Glass containing ~8.7 wt% MoO_3 was successfully manufactured without any operational problems on the VTR, indicating that the existing plant can be used to vitrify high molybdenum feeds without any modifications. The glass manufactured on the VTR was considered to be of good quality.

Acknowledgements

The Authors would like to thank Sellafield Ltd for sponsoring this work on behalf of the Nuclear Decommissioning Authority.

References

1. B. F. Dunnett, N. R. Gribble, R. Short, C. J. Steele and A. D. Riley, Glass Technol.: Eur. J. Glass Sci. Technol. A, 53, 166 (2012)

2. Werner Lutze, in Radioactive Wasteforms for the Future, edited by W. Lutze and R. Ewing (North Holland, Amsterdam, 1988), ISBN 0444871047, pp. 31-32.

3. B. Dunnett, N. Gribble, A. Riley and C. Steele, Mat. Res. Soc. Symp. Proc., 1193, 291, (2009).

4. M. I. Ojovan, W.E. Lee. 'An Introduction to Nuclear Waste Immobilisation', Elsevier, Amsterdam, ISBN 0080444628 (2005).

5. N. Henry, P. Denlard, S. Jobic, R. Brec, C. Fillett, F. Bart, A. Grandjean, O. Pinet, Journal of Non-crystalline Solids, 333, 199, (2004).

6. R. Do Quang, V. Petijean, F. Hollebecque, O. Pinet, T. Flament and A. Prod'homme, 'Vitrification of HLW produced by uranium/ molybdenum fuel reprocessing in Cogema's cold crucible melter', WM'03 Conference, February 23-27, Tucson, AZ (2003).

7. I.A. Sobolev, S.A. Dmitriev, F.A. Lifanov, A.P. Kobelev, S.V. Stefanovsky and M.I. Ojovan, Glass Technology, 46, 28, (2005).

8. M.I. Ojovan and W.E. Lee, 'New Developments in Glassy Nuclear Wasteforms', Nova Science Publishers, New York, ISBN 9781600217838 (2007).

9. K. Bradshaw, N. R. Gribble, P. A. Mayhew, M. C. Talford and A. D. Riley, "Full Scale Non-Radioactive Vitrification Development in Support of UK Highly Active Waste Vitrification", Proceedings of Waste Management Symposium, (2006).

EFFECT OF COMPOSITION OF UK VITRIFIED HLW ON LONG-TERM DURABILITY

Mike Harrison
mike.t.harrison@nnl.co.uk

INTRODUCTION

In the UK, highly radioactive liquor (HAL) from the reprocessing of spent nuclear fuel is converted into a borosilicate glass at the Sellafield Waste Vitrification Plant (WVP) yielding a stable and durable wasteform suitable for long-term storage and subsequent disposal. There are two distinct types of HAL feed that arise from the reprocessing of Magnox (uranium metal) and Oxide (Advanced Gas-cooled Reactor (AGR), and Light Water Reactor, (LWR) uranium oxide ceramic) spent fuel. Magnox HAL contains significant amounts of Mg and Al, while Oxide HAL lacks these elements, but is generally of higher burn-up and so has higher fission product content along with other process additives such as Gd. In order to ensure that the product from vitrification of Oxide HAL complies with the requirements of the process specification, the Oxide feed has to be blended with Magnox HAL. Currently, the 'standard' Blend ratio is 3:1 Oxide:Magnox on the basis of the weight of equivalent metal oxides in the HAL, which is generally referred to in percent terms as '75o:25m' where 'o' and 'm' refer to Oxide and Magnox respectively. If the Oxide content is >80% then the product will have unacceptable aqueous durability due to the lack of aluminium. Lower Oxide to Magnox ratios, e.g. 50o:50m, are likely to be implemented on WVP using the current 'MW' (Mixed Windscale) base glass formulation in the near future.

WVP product glass is manufactured to a quality assured process specification (QAPS), with an historic targeted waste oxide incorporation of 25 wt% for both Magnox-only and Blend HAL feeds, i.e. the weight ratio of 'MW' base glass to waste on an equivalent metal oxide basis is 3:1. Recently, however, by using the full-scale inactive Vitrification Test Rig (VTR) it has been possible to determine operational envelopes for higher waste loadings. This will result in fewer containers for both storage and disposal. Waste loadings up to 35 wt% have been demonstrated on the VTR for both Magnox and Blended feeds. As a result of the qualification work on the VTR, higher incorporations have now been implemented on WVP, with the targeted waste oxide loadings for Magnox and 75o:25m Blend glasses in recent campaigns being 32 and 28 wt% respectively.

As part of the product qualification process, it is required that any new compositions fabricated on WVP have aqueous durability of a similar order to the 'standard' 25 wt% loading of Magnox only and of 75o:25m Blend glasses. To this end, all new compositions undergo a static leach test based on the ASTM Product Consistency Test (PCT) protocol (1) to compare their relative longer-term behaviour with that of the 'standard' 25 wt% glasses. Following on from the initial PCT studies of higher incorporations (2), these tests were extended out to longer durations with a wider range of compositions (3).

Table 1 shows the glass compositions that underwent long-term durability tests in order to investigate the effect of varying waste loading. Note that the majority of the glasses were fabricated at full scale on the VTR and are, therefore, generally representative of the WVP vitrified product.

Table 1: Summary of glasses investigated in long-term durability tests

	Waste Loading / wt%	*Waste Type*	*Li_2O / wt%*	*Lab or VTR glass*
1	25	Magnox	4.0	Lab
2	28	Magnox	3.8	VTR
3	28 + 1% Li_2O	Magnox	4.8	VTR
4	32	Magnox	3.6	VTR
5	35	Magnox	3.5	VTR
6	38	Magnox	3.3	VTR
7	17	75o:25m Blend	4.0	VTR
8	31	75o:25m Blend	3.7	VTR
9	38	75o:25m Blend	3.5	VTR

All of the samples in Table 1 were fabricated from 'MW' base glass (22.4 B_2O_3, 5.4 Li_2O, 11.0 Na_2O and 61.2 SiO_2 wt%) melted with calcined HAL simulant. As the waste loading was increased, the proportion of 'MW' and, hence, the Li_2O content, decreased. However, on WVP a portion of the lithium required in the final glass product is added to the HAL in order to optimise the calcination process. The presence of lithium in the HAL prevents the formation of refractory oxides during the calcination process that would otherwise be slow to react with the glass in the melter. For 25 wt% incorporation, this results in a 50:50 split of the Li between the HAL and a modified base glass ('MW-½Li') to give the required total Li_2O content of 4 wt% and an ideal target Li:Na mole ratio of 1. However, this strategy has resulted in WVP vitrified product with variable Li_2O contents and deviations from an equimolar Li:Na ratio. In particular, waste loadings >25 wt% have, historically, yielded HLW glass with >4 wt% Li_2O, which could potentially be detrimental to glass durability. The alkali metals act as glass structure modifiers breaking up the silicate network. This reduces the viscosity to ensure rapid reaction between the molten glass and calcine and easy pouring of the melt at ~1050 °C. Furthermore, having an equi-molar amount of Li and Na was found to optimise a number of glass properties, e.g. viscosity, waste incorporation and durability, as a result of the improved packing efficiency from the different ionic radii (the 'mixed-alkali' effect). However, too much alkali makes the glass more susceptible to chemical attack by water through the ion-exchange process; hence, the durability is reduced.

Following the testing of glass 3 in Table 1 it was noted that the precise lithium concentration in the glass has a significant influence on the aqueous durability. Hence, a more systematic study of the effect of lithium on the long-term durability was carried out by testing the compositions shown in Table 2 using the same standard PCT protocol (3).

Table 2: Magnox glass compositions used to study the effect of Li_2O concentrations >4 wt%

	Waste Loading / wt%	*Li_2O concentration / wt%*	*Li:Na Ratio*	*Total Alkali Content (Li+Na+Cs mol%)*
i	25	4.0	1.01	10.53
ii	25	4.5	1.14	11.10
iii	25	5.0	1.28	11.66
iv	32	4.0	1.12	10.57
v	32	4.5	1.27	10.96
vi	32	5.0	1.42	11.53

Experimental

To prepare the leach test powders, glass samples were crushed, milled, and then sieved to obtain the 75 – 150 µm size fraction. This powder was then washed to remove fines and dried at 90 °C according to the ASTM procedure (1).

The PCTs were carried out in triplicate with 4 g of glass and 40 mL de-ionised water in PFA (Polyfluoroalkoxy) screw-lidded jars. This gave a surface-area to volume (*S/V*) ratio of ~2,000 m^{-1}. Tests were put in an oven at 90 °C for durations of 7, 14, 21, 28, 42, 56, 84 and 112 days. Upon removing from the oven, the leach test vessels were allowed to cool and a sample of the leachate taken for elemental analysis via ICP-OES.

From the B, Li, Mg, Mo, Na and Si concentrations in the leachates, the normalised elemental mass losses *NL(i)* were calculated according to the equation:

$$NL(i) = \frac{c_i}{f_i(S/V)}$$

where c_i is the concentration of element *i* in the leachate in ppm, f_i is the mass fraction of element *i* in the unleached wasteform, and *S/V* is the surface area to volume ratio in m^{-1}. The normalised boron mass loss *NL(B)* is used as an indicator for general glass dissolution as boron has simple solution chemistry and is not involved in the formation of any secondary alteration phases.

Results and Discussion

The *NL(B)* values as a function of duration for the Magnox glasses in Table 1 are compared in Figure 1. With the exception of the 28 wt% glass with an extra 1 wt% Li_2O, there is a steady decrease in the *NL(B)* values as the waste incorporation is increased. In addition, the *NL(B)* response up to 112 days is consistent with that previously reported for 25 wt% Magnox glasses under similar test conditions (4, 5), i.e. a rapid initial release followed by a decrease in rate to a much lower value. These are known as the 'initial' and 'residual' rate regimes respectively and are observed for the majority of borosilicate HLW glasses dissolved in static aqueous conditions (5, 6).

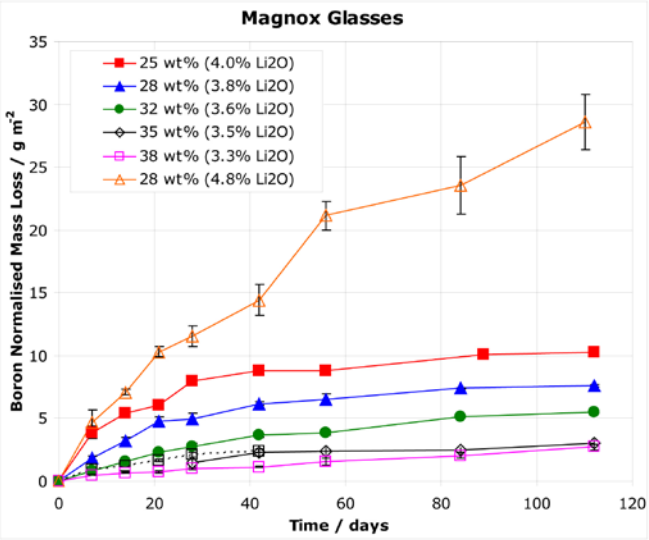

Figure 1: Comparison of normalised boron mass loss NL(B) for Magnox glasses. The dotted line for 31 wt% represents the data from the earlier experiments performed up to 42 days (2).

However, the 28 wt% glass with the extra 1% Li_2O shows significantly higher *NL(B)* values and a lack of any obvious approach to a residual rate. This result shows that the amount of Li in the glass can have a significant effect on its durability.

Figure 2 compares the normalised boron mass losses for the Blend glasses in Table 1. Although the leach tests completed for Blend glasses were not as extensive as for Magnox, there is a similar trend with the *NL(B)* values generally decreasing as the waste incorporation increases. Compared to Magnox glasses, the reduction in boron release rate from initial to residual is much more marked, with *NL(B)* reaching a near constant value after 42 days for the 31 and 38 wt% waste incorporations. The low incorporation (17 wt%) Blend glass does show different behaviour with higher residual rate between 42 and 112 days.

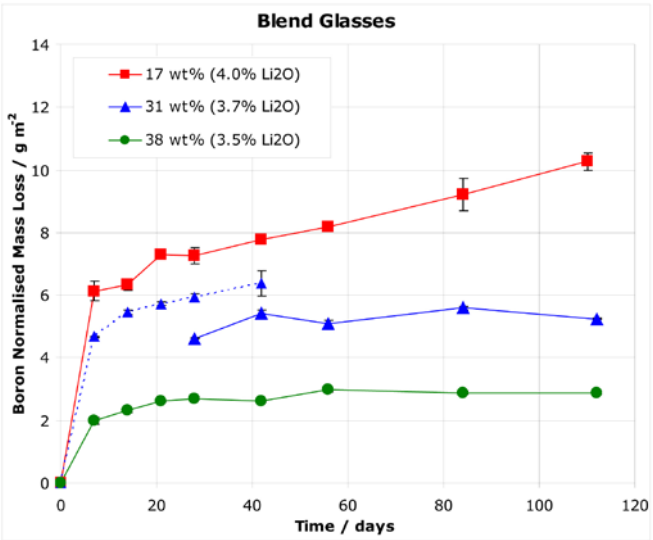

Figure 2: Comparison of normalised boron mass loss NL(B) for 75o:25m Blend glasses fabricated on the VTR. The dotted line for 31 wt% represents the data from the earlier experiments performed up to 42 days (3)

Higher incorporation 75o:25m Blend appears to behave very favourably when compared to the Magnox glasses. This will be related to the concentrations of key species such as Mg, Al, B, and the alkali metals in the various compositions. However, deconvoluting the effects of the different elements in these multi-component glasses is extremely complex. For example, magnesium is often cited as being detrimental to glass durability (6). The better performance of Blend glasses, which typically have a third of the magnesium content of Magnox glasses, appears to corroborate this. However, Blend glasses also have a third of the aluminium content, which would be expected to worsen the durability. Furthermore, increasing the waste incorporation appears to improve the durability for both Magnox and Blend glasses, despite the higher Mg concentration. This may simply be due to the decreasing lithium concentration as waste loading is increased, but other waste components, such as iron, are also likely to have an effect.

Figure 3 compares the normalised boron mass losses for the 25 and 32 wt% Magnox glasses with varying Li_2O content from Table 2 tested at 90 °C in DIW for 112 days with a *S/V* ratio of ~2,000 m^{-1}. In general, for a given waste loading, as the lithium content is increased, *NL(B)* increases. However, a number of other important observations can be made:

- For both 25 and 32 wt% Magnox glasses, the increase in *NL(B)* values on going from 4.0 to 4.5 wt% lithia is significantly more marked than on going from 4.5 to 5.0 wt%.
- For 32 wt% Magnox, the increase in *NL(B)* values on going from 4.0 to 4.5 or 5.0 wt% lithia is significantly more marked than for 25 wt%.

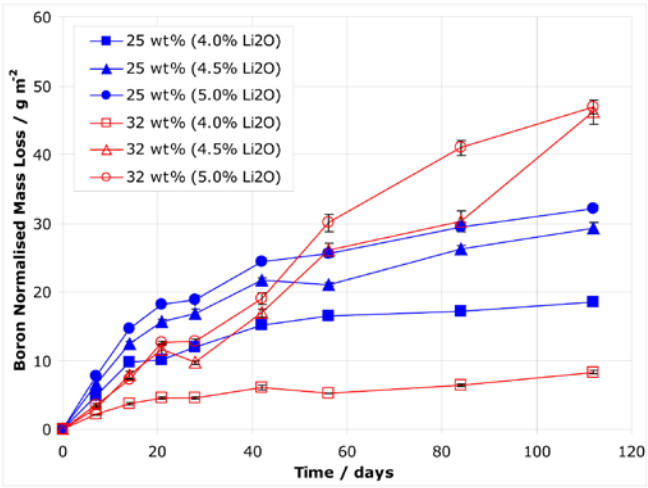

Figure 3: Comparison of the normalised boron mass losses for 25 and 32 wt% Magnox glasses with 4.0, 4.5 and 5.0 wt% Li_2O

Hence, it can be seen that the precise effect of increased lithia content in Magnox glasses also depends on the waste loading. For example, the 25 wt% Magnox glass appears relatively insensitive to increasing the Li_2O from 4.0 to 5.0 wt%, whereas for the 32 wt% Magnox glass it increases the *NL(B)* values markedly.

CONCLUSIONS

A number of compositional variations for simulated UK HLW glasses have been studied using static powder leach tests at 90 °C in DIW based on an ASTM standard procedure.

For Magnox glasses, the normalised boron mass loss decreases as the waste incorporation is increased. The dissolution behaviour also depends on the lithium concentration in the glass, with normalised mass losses generally increasing with increased Li_2O content. This is generally to be expected as an effect of the increased alkali metals in the glass. However, the precise behaviour is complex, with the sensitivity to increases in lithium concentration from 4.0 to 5.0 wt% also depending on the waste incorporation.

For Blend glasses, the *NL(i)* values are lower at all waste incorporations than their Magnox counterparts. Furthermore, the release rates reduce to an apparent low 'residual' value after a relatively short time, with the exception of low incorporation Blend (<20 wt%), which seems to dissolve faster under the test conditions studied.

For both Magnox and Blend glasses this study showed that, under the test conditions used, increasing the waste incorporation in vitrified HLW is not detrimental to chemical durability. Indeed, the normalised mass losses reduced as the proportion of waste in the glass was increased. However, care needs to be taken with the lithium-dosing strategy in WVP for Magnox glasses as increased Li_2O content was detrimental to glass durability, especially at higher waste loadings, e.g. 32 wt%. Hence, it was recommended that for all waste loadings, WVP should target a Li:Na ratio of 1:1 and Li_2O content ≤4 wt%.

Acknowledgements

The author would like to thank Sellafield Ltd and in particular Carl Steele for sponsoring this work.

References

1. ASTM C1285-02: "Standard Test Methods for Determining Chemical Durability of Nuclear, Hazardous, and Mixed Waste Glasses and Multiphase Glass Ceramics: The Product Consistency Test (PCT)".

2. C. Brooks, M. Harrison, A. Riley and C. Steele "The Effect of Increased Waste Loading on the Durability of High Level Waste Glass", *Mater. Res. Soc. Symp. Proc.*, **1265**, 109, (2010).

3. Mike T. Harrison, Carl J. Steele & Andrew D. Riley "The effect on long term aqueous durability of variations in the composition of UK vitrified HLW product", *European Journal of Glass Science and Technology A: Glass Technology*, **53**, 211, (2012).

4. H. U. Zwicky, B. Grambow, C. Magrabi, E. T. Erne, R. Bradley, B. Barnes, Th. Graber, M. Mohos and L. O. Werme "Corrosion behaviour of British Magnox waste glass in pure water", ***Mat. Res. Soc. Symp. Proc.***, **127**, 129, (1989).

5. E. Curti, J. L. Crovisier, G. Morvan, and A. M. Karpoff "Long-term corrosion of two nuclear waste reference glasses (MW and SON68): A kinetic and mineral alteration study", *Applied Geochemistry*, **21**, 1152, (2006).

6. P. Frugier, S. Gin, Y. Minet, T. Chave, B. Bonin, N. Godon, J.-E. Lartigue, P. Jollivet, A. Ayral, L. De Windt and G. Santarini "SON68 nuclear glass kinetics: Current state of knowledge and basis of the new GRAAL model", *Journal of Nuclear Materials*, **380**, 8, (2008).

HOT ISOSTATICALLY PRESSED NUCLEAR WASTEFORMS FOR THE FUTURE

Ewan Maddrell
ewan.r.maddrell@nnl.co.uk

INTRODUCTION

The two best established waste immobilisation technologies in the UK nuclear industry are cementation and vitrification. Cementation is used for the encapsulation of a wide variety of intermediate level wastes using blends of ordinary Portland cement with either blast furnace slag or pulverised fly ash. Vitrification is used for the immobilisation of high level waste from both the UK Magnox and THORP spent nuclear fuel reprocessing plants. The diversity of wastes that exist on the Sellafield site means that many fall outside the envelope for these two processes and require the development of new immobilisation technologies. Hot isostatic pressing (HIP) represents a powerful emerging technology that offers a route for the immobilisation of orphan waste streams and also has the potential to meet wasteform requirements for future nuclear fuel cycles (1).

In HIP the waste is typically mixed with an appropriate precursor and the blended material is fed into a specially designed can, which is then evacuated and sealed. The sealed can is subjected simultaneously to elevated temperature and isostatic pressure, typically 50-100 MPa of argon, to consolidate the waste and precursor blend into a monolithic wasteform. Pilot plant scale HIP cans, before and after consolidation, are shown in Figure 1. Before consolidation the body of the HIP can shown is 0.25 m high by 0.2 m diameter. The enclosed volume is reduced on consolidation by 50 to 60 %. HIP cans of this design have been made up to 1.5 m high and 0.7 m diameter.

Figure 1: Pilot scale HIP cans before (right) and after (left) consolidation

Key advantages of HIP technology include:

- A wide processing window and generates minimal secondary wastes.
- Insensitivity to the physical, electrical and thermal properties of the wasteform.
- Batch processing, material inventory accountancy/criticality control is simplified.
- Totally contained consolidation process with no potential for volatile losses.
- Is scale independent.

The immobilisation of Pu residues

Plutonium residues are a category of materials stored on the Sellafield site that are incompatible with current waste immobilisation technology. The material is of a disparate nature and span compositions with Pu contents just in excess of that permitted for classification as Pu contaminated material, through to separated but impure Pu that cannot economically be returned to the fuel cycle.

To meet the immobilisation requirements a suite of wasteforms is to be used with their compositions tailored to meet certain needs. For residues with low Pu contents a glass ceramic wasteform is used. The principle behind the wasteform is that the Pu partitions into crystals of the mineral zirconolite ($CaZrTi_2O_7$) whilst the balance of the waste is incorporated into the glass matrix. The microstructure of a typical glass ceramic wasteform, imaged by scanning electron microscopy, is shown in Figure 2. Material that can be classified

as impure Pu does not require a wasteform with the flexibility conferred by a glass matrix and can be immobilised in a fully ceramic wasteform of the same zirconolite phase. Zirconolite is also the preferred phase should a portion of the UK's stockpile of separated Pu require immobilisation. The majority of the residues, by mass, is comprised of mixed U and Pu oxides that remain from the UK's fast reactor programme in the form of powder, green pellets and sintered pellets. This material would be compatible with a zirconolite wasteform but at an uneconomic waste loading. Significantly higher waste loadings can be achieved using a related Ti-pyrochlore phase based on the mineral betafite ($CaUTi_2O_7$). The power of hot isostatic pressing is such that the three wasteforms can be produced using the same HIP unit and same design of HIP cans. (2)

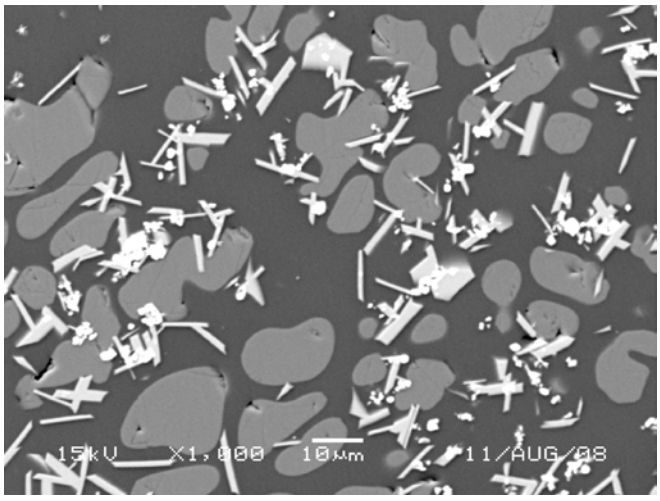

Figure 2: Microstructure of glass ceramic wasteform. Black is glass matrix; dark grey is CaF_2 used as a waste simulant; light grey is zirconolite; white is free ZrO_2

A pilot facility for the immobilisation of plutonium residues, sited in NNL's Central Laboratory, is currently being designed with active commissioning expected to begin in 2017.

Hot isostatic pressing for future fuel cycles

With the anticipated renaissance of nuclear power in the UK comes the challenge of managing the associated waste. There are many arguments in support of the chemical treatment of spent nuclear fuel, which include being able to recycle valuable fissile and fertile materials and as a means to optimise the management of the waste for repository disposal. Possible improvements to spent fuel recycling include total dissolution of fuel assemblies using electrochemical techniques. This is much less mechanically intensive than current methods but leads to a highly active waste stream rich in the metals of fuel assembly construction, such as Zr, Fe, Ni and Cr. This stream is incompatible with vitrification technology because the oxides of these metals are very refractory. An alternative immobilisation method lies with the use of ceramic wasteforms, which allow some of the components of the waste to become functional constituents of the wasteform. The composition of these wasteforms means that they are best consolidated using HIP. Differences in fuel assembly design lead to variations in the composition of the highly active waste, and the waste compositions from eight fuel assemblies, normalised to 1 tonne of initial fuel are shown in Table 1. It has been shown that a common precursor composition can be used to immobilise all of the waste arisings (3).

Table 1: Normalised Fuel Assembly Data per Tonne Fuel (Pre-Irradiation; (kg)

Fuel Assembly	A	B	C	D	E	F	G	H
Fe_2O_3	43.64	33.32	71.71	31.51	37.80	42.22	38.35	42.99
Cr_2O_3	12.53	12.93	24.31	12.38	15.52	12.10	11.01	13.02
NiO	4.98	14.75	20.98	14.38	19.46	4.82	4.37	7.17
Minor Oxides	1.11	2.76	4.06	2.67	3.60	1.08	0.98	1.49
ZrO_2	74.34	53.02	58.76	54.19	62.08	65.74	65.14	67.41
SnO_2	1.07	0.76	0.84	0.78	0.89	0.95	0.94	0.97
Fission Products	57.90	57.90	57.90	57.90	57.90	57.90	57.90	57.90
Gd_2O_3	9.10	9.10	9.10	9.10	9.10	9.10	9.10	9.10
Actinides	3.30	3.30	3.30	3.30	3.30	3.30	3.30	3.30
Total	207.97	187.82	250.97	186.22	209.65	197.21	191.09	203.36
Mass Precursor	250.97	250.97	250.97	250.97	250.97	250.97	250.97	250.97
Waste form mass	458.94	438.79	501.93	437.18	460.61	448.18	442.06	454.33
Waste volume (m^3)	0.102	0.098	0.112	0.097	0.102	0.100	0.098	0.101
Waste loading (%)	45.3	42.8	50.0	42.6	45.5	44.0	43.2	44.8

The wasteform is derived from Synroc but the use of waste components in the wasteform means that waste loadings up to 50 wt% are achieved. The wasteform is composed of ceramic phases based on natural minerals: zirconolite ($CaZrTi_2O_7$); redledgeite ($BaCr_2Ti_6O_{16}$); loveringite ($Ca(Ti,Fe,Cr)_{21}O_{38}$) and perovskite ($CaTiO_3$). The fission products and non-recycled minor actinides are immobilised by incorporation as solid solutions within these phases. The chemical flexibility of the wasteform is achieved through subtle variations in the composition and abundance of the above phases. A typical microstructure of the wasteform is shown in Figure 3.

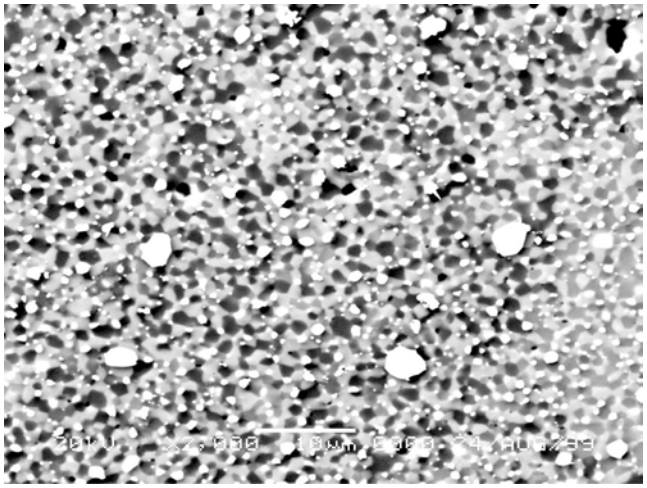

Figure 3: Microstructure of ceramic wasteform for possible future nuclear fuel recycling applications. The chemical variations of the phases are reflected by their different levels of brightness

One of the main challenges for a future fuel cycle is the impact of decay heat on the repository environment. This is expected to lead to a requirement for extended periods of surface storage. Conceptually, one method to achieve this is through partitioning and selective immobilisation of the highly active waste. This allows the heat generating radionuclides, primarily Cs and Sr, to be immobilised in a dedicated wasteform. The decay heat means that typical glass compositions are vulnerable to devitrification, and ceramic wasteforms derived from the phases mentioned above are advantageous. In addition to providing a route to consolidation, HIP also prevents volatilisation of Cs and its compounds, and facilitates the necessary redox control for fission product incorporation in the host phases.

The stabilisation of ion exchange compounds

Synthetic inorganic ion exchange compounds provide an example of a material ideally suited to stabilisation by HIP. Ionsiv is based on a silicotitanate framework substituted with Nb to improve its ion exchange properties. The functional ion exchange component is then formed into millimetre sized spheres using a Zr-based binder. The most high profile application of Ionsiv has been to remove Cs from contaminated water at the Fukushima Daiichi nuclear power plant in Japan.

The formulation of Ionsiv is serendipitous, not simply that it is amenable to thermal conversion with no additives, but because it forms durable Cs host phases on conversion (4). A typical microstructure of thermally converted Ionsiv is shown in Figure 4; the fine grain size makes it impossible to determine the composition of individual grains using scanning electron microscopy combined with energy dispersive spectroscopy.

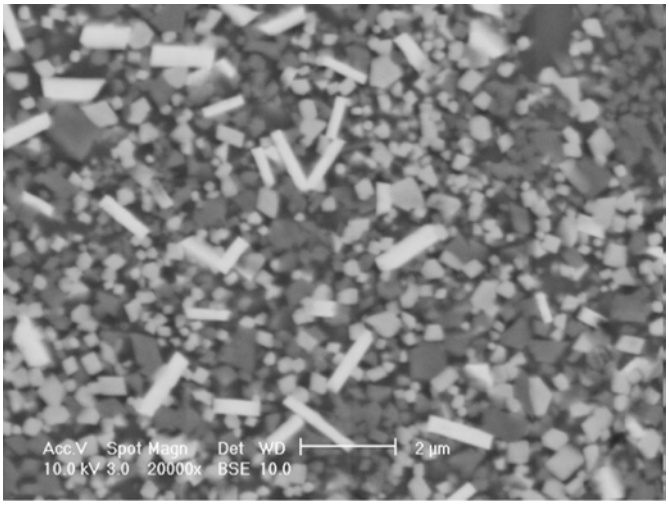

Figure 4: Microstructure of thermally converted Ionsiv IE-911

Working in collaboration with the University of Birmingham the thermal conversion process has become better understood. This is illustrated in Figure 5 as a series of X-ray diffraction (XRD) spectra progressing from Cs free Ionsiv to Cs loadings of 4, 8 and 12 wt%. For clarity, only the diffraction peaks corresponding to the Cs host phases are indicated. The Cs free sample shows neither of the host phases. At 4 wt% Cs the formation of $Cs_2TiNb_6O_{18}$ is observed. At 8 wt% Cs a second Cs host phase, $Cs_2ZrSi_6O_{15}$ can be seen, and the intensity of this phase is increased at 12 wt% Cs. Note that both phases contribute to the peak just above 26° and this is reflected in the different ratio of peak heights for the doublet around 26° in the 8% Cs and 12% Cs traces. XRD from intermediate compositions add to the picture that $Cs_2TiNb_6O_{18}$ is the preferred Cs host phase and forms until the Nb is exhausted. Thereafter further Cs is immobilized in the $Cs_2ZrSi_6O_{15}$ phase. A simple mass balance exercise based on the analysed compositions of these samples supports this picture.

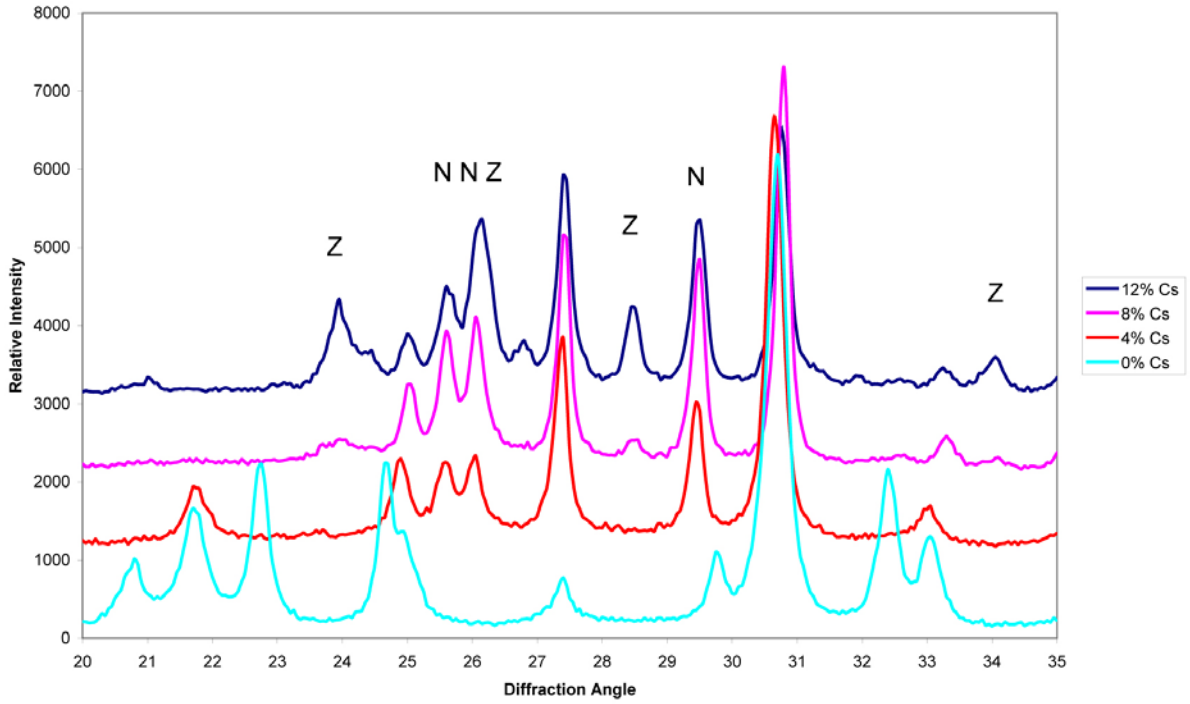

Figure 5: X-ray diffraction spectra of thermally converted Ionsiv showing ingrowth of Cs host phases with increasing Cs content. N represents $Cs_2Nb_6TiO_{18}$; Z represents $Cs_2ZrSi_6O_{15}$

Thermal conversion of Ionsiv is an attractive alternative to immobilisation by cementation or vitrification. Cementation is problematic because the radiogenic heating from the Cs will dehydrate the wasteform and lead to its disintegration. Vitrification is more thermally tolerant, but the Ti, Nb and Zr content of the Ionsiv mean that only very low waste loadings can be achieved. By contrast, with thermal conversion the waste loading is effectively 100 % and because the wasteform is made by a thermal process it is tolerant of the radiogenic heating. The application of HIP means that Ionsiv stabilisation at the 10 – 100 kg scale can be carried out.

CONCLUSIONS

Hot isostatic pressing is an emerging wasteform consolidation technology that is finding its first applications in niche areas for wastes that are unsuitable for the mainstream immobilisation technologies. As acceptance of HIP as a waste immobilisation technology grows it has the potential to surpass vitrification and cementation by delivering wasteforms with reduced volumes and improved durability.

References

1. Maddrell, E.R., "Hot isostatically pressed wasteforms for future nuclear fuel cycles", *Chem. Eng. Res and Des.*, **91**, 735, (2013).

2. Scales, C.R., E.R. Maddrell, J.W. Hobbs, R.G. Stephen, S.S. Moricca and M.W.A. Stewart, "Building flexibility into the design of a pilot plant for the immobilisation of Pu containing residues and wastes", The 15th International Conference On Environmental Remediation And Radioactive Waste Management, ASME (2013).

3. Maddrell, E.R., "Generalized Titanate Ceramic Waste Form for Advanced Purex Reprocessing", *J. Am. Ceram. Soc.*, **84**, 1187, (2001).

4. Chen, T.-Y., J.A. Hriljac, A.S. Gandy, M.C. Stennett, N.C. Hyatt and E.R. Maddrell, "Thermal Conversion of Cs-exchanged IONSIV IE-911 into a Novel Caesium Ceramic Wasteform by Hot Isostatic Pressing", in "Scientific Basis for Nuclear Waste Management XXXVI", MRS Proc **1518** (2013).

STRONTIUM 90 MOBILITY IN CONTAMINATED NUCLEAR FACILITIES AND GROUNDWATER

Joe Small[1], Sarah Wallace[2] and Ian Burke[2] *1 NNL, 2 University of Leeds*
joe.s.small@nnl.co.uk

INTRODUCTION

Strontium-90 (^{90}Sr) is a beta emitting radionuclide produced during nuclear fission and is a soil and groundwater contaminant at many nuclear facilities globally. With a half life of 29.9 years ^{90}Sr ground contamination will need to be managed for several hundred years. Understanding the mechanism of ^{90}Sr retention in engineered and natural environments will be a key input to decision making regarding site remediation. The mobility of ^{90}Sr in these environments is controlled either by sorption to sediment particles or incorporation reactions into secondary mineral precipitates. These subsurface processes are influenced by natural groundwater compositions and anthropogenic liquors that may be associated with releases of ^{90}Sr. At the Sellafield site ^{90}Sr is the predominant beta-emitting contaminant in groundwater and is potentially sourced from a range of waste storage facilities, including neutralised nitrate containing wastes and silos containing corroded Magnox fuel cladding comprising $Mg(OH)_2$ and buffered at pH 9 to 11.5. The Separation Area of the Sellafield site comprises a large amount of concrete, either in the foundations of original silos or as ground cover. Alkaline cementitious leachate related to such silos and construction has the potential to affect the sorption and retention of ^{90}Sr. Research at the US Department of Energy Hanford site has highlighted how highly caustic leak solutions (containing Na^+. NO_3^- and Al^{3+}) have the potential to form a range of secondary zeolite phases, which can accommodate Sr^{2+} and Cs^+. Once released from source, transport of ^{90}Sr in groundwater is primarily controlled by sorption reactions with sediments that are affected by geochemical conditions, sediment mineralogy and groundwater composition/salinity. Such factors will be of significance to understand the fate of ^{90}Sr contamination in the saline interface recently highlighted by leakage to ground of cooling water following the Fukushima accident. This paper provides a summary of research undertaken to explore the mechanism of ^{90}Sr sorption and retention on sediments representative of the Sellafield site under a range of relevant anthropogenic and natural chemical conditions.

Materials and Methods

Batch experiments were performed in triplicate to test the influence of pH, ionic strength (IS) and mineral alteration on the degree of ^{90}Sr sorption to sediments representative of the quaternary deposits that underlie the UK Sellafield site. The sediment was a fine grained silty sand (3 ± 1 % clay), where clay minerals and iron oxides coat the sand grains and are expected to provide the main substrate for Sr sorption. Chlorite ($Mg_5Al(AlSi_3)O_{10}(OH)_8$) was the dominant clay mineral with minor amounts of illite ($(K,H_3O)(Al,Mg,Fe)_2(Si,Al)_4O_{10}(OH)_2$) and iron(III) oxides (hematite and goethite) also detected. The sediment contained ~0.5 % organic carbon. The natural Sr content was 56 mg/kg, which was non-exchangeable and associated with mineral phases.

Sorption experiments considered the following range of regional groundwater and anthropogenic liquor compositions that have particular relevance to Sellafield and other UK sites:

A. HNO_3 groundwater (pH 3.5, IS 8 mmol/L)
B. Unbuffered groundwater (pH 5.5, IS 8 mmol/L)
C. HCO_3^- buffered groundwater (pH 7,2, IS 8 mmol /L)
D. Magnox tank liquor (pH 11, IS 29 mmol/L)
E. Young cement water (YCW), representing initial bleed from cement dominated by KOH, with NaOH, Na_2SO_4 and saturated with $Ca(OH)_2$ (pH 13.5, IS 0.55 mmol/L)

For measurement of the amount of ^{90}Sr sorbed, dried sediment was reacted with groundwater solutions A-E at room temperature (21°C) in 100 ml HDPE Erlenmeyer flasks using a solid : solution ratio of 100 g/L (Fig 1) All sediments were left to equilibrate with groundwaters (under inert atmosphere) for 24 h then spiked with ^{90}Sr tracer to a final specific activity of 30 Bq/mL (5.9×10^{-9} mol/L). Using radioactive ^{90}Sr tracer allowed experiments to be carried out at environmentally relevant concentrations, similar to those found in Sellafield contaminated land. After spiking, each flask was agitated and samples

were withdrawn at 1, 4, 24 and 48 hours after ^{90}Sr addition. The aqueous concentration of ^{90}Sr was determined by liquid scintillation counting (LSC). The % ^{90}Sr sorbed was calculated as follows:

$$\%^{90}Sr_{sorb} = \frac{A_i - A_e}{A_i} \times 100$$

Where A_i = initial added activity (Bq/mL), A_e = activity after sorption (Bq/mL).
The effect of pH variation was determined, in additional sorption tests, using the artificial unbuffered groundwater solution (Solution B) as the background electrolyte. A pH titration over a pH range of 2 - 10 was achieved in replicate experiments by addition of progressively more concentrated HCl or NaOH solutions. Similarly the effect of Ca^{2+} and Na^{+} competition was investigated in the bicarbonate buffered groundwater solution (pH 7.2) by addition of progressively more concentrated $CaCl_2$, and NaCl solutions respectively (0.1×10^{-4} - 0.1 mol/L). The solutions and sediments were mixed for 24 hours prior to spiking with ^{90}Sr tracer, after 48 hours agitation at 125 rpm, pH and ^{90}Sr activity was determined as above.

Long-term sorption experiments were undertaken to examine Sr^{2+} interaction over periods of 10, 30, 90 and 365 days. Experiments were performed in HCO_{3-} buffered groundwater, Magnox tank liquor and YCW with 20 ppm stable Sr^{2+} and a lower solid solution ratio (20 g/L) in order that sufficient solid could be produced for X-ray absorption spectroscopy (XAS) characterisation of the Sr speciation. In addition a further young cement water (YCW) experiment (pH 13.5) was performed at an elevated temperature 70°C for 365 days.
Sr K-edge XAS spectra were collected at beamline BM26a at the European Synchrotron Radiation Facility, Grenoble. Extended X-ray absorption fine edge structure (EXAFS) were analysed to provide information on the near neighbour coordination of the sorbed Sr. Sequential extraction techniques were used to progressively leach the Sr from the sediments using 1 mol/L $MgCl_2$ (pH 7, 2 hours), 1 mol/L sodium acetate (pH 5, 5 hours) and finally 0.5 mol/L hydroxylammonium chloride (acid pH 1.5, 12 hours). Between each stage the supernatant after centrifugation and filtration was analysed for ^{90}Sr by LSC. Mineralogical changes were characterised using powder X-ray diffraction (XRD), scanning electron microscopy (SEM) with energy dispersive X-ray analysis (EDX) and electron microprobe techniques.

Figure 1: Batch experiment setup used in this study. Experiments used ^{90}Sr tracer to measure Sr sorption

^{90}Sr sorption and effect of pH and ionic strength

Strontium uptake to the sediment was rapid in all experimental groundwaters with the majority of ^{90}Sr sorption occurring within 4 hours. After this time there was only a small increase in ^{90}Sr sorption measured at 24 hours and 48 hours in all groundwater systems. Sorption of ^{90}Sr in the low ionic strength (~ 8 mmol/L) groundwater systems (A-C) varied widely (Fig 2), but with a clear pH dependence. At pH 3.5 in the nitric acid affected groundwater (A) only 29 % ^{90}Sr was sorbed after 48 hours. In the unbuffered (pH 5.5) and bicarbonate buffered (pH 7.2) groundwater the degree of sorption increased significantly, to 61.8 % and 98.9 % ^{90}Sr sorption respectively. This pH related "sorption edge" was also evident in experiments where the unbuffered groundwater pH was titrated (Fig 2 crosses), which correlate well with the trend for the groundwater compositions A-C.
Sorption of ^{90}Sr in the pH 11 artificial Magnox tank liquor (D) (ionic strength 29.2 mmol/L) was notably lower (~ 79 %) than the bicarbonate groundwater system (Fig 2). Experiments examining the effect of increasing concentration of Na^{+} and Ca^{2+}, which compete with Sr^{2+} for sorption, indicate a reduction in the amount of ^{90}Sr sorption occurs above a total IS of 5 mmol L^{-1} (Fig 3). To further confirm this effect geochemical speciation modelling was undertaken with the PHREEQC code, where the sorption processes were represented by a cation exchange model that considers competing exchange with Na^{+}, K^{+}, Ca^{2+} and Mg^{2+}. The PHREEQC model simulates the trend in the ionic strength effect, a fitted model is plotted in Fig 3 where the concentration of exchange sites was increased to 30 milli equivalent per 100g (meq/100 g) from the measured cation exchange capacity of the original sediment (8.2 ± 5.1 meq/100 g) and

small adjustments were made to the exchange coefficients for Na^+, Ca^{2+} and Sr^{2+}. With these adjustments to the ion exchange model and the consideration of a possible surface complexation model for Sr^{2+} sorption onto iron hydroxides, the very high levels of sorption measured at low ionic strength are not fully represented by the model. This enhanced sorption behaviour was not observed in previous Sr sorption studies of Sellafield sediments undertaken by NNL that used sediments with generally much lower organic matter content (< 0.1 % versus 0.56 %). We therefore tentatively suggest that the higher total adsorption observed in this study is due to enhanced Sr^{2+} sorption to organic matter that is not captured by the cation exchange model.

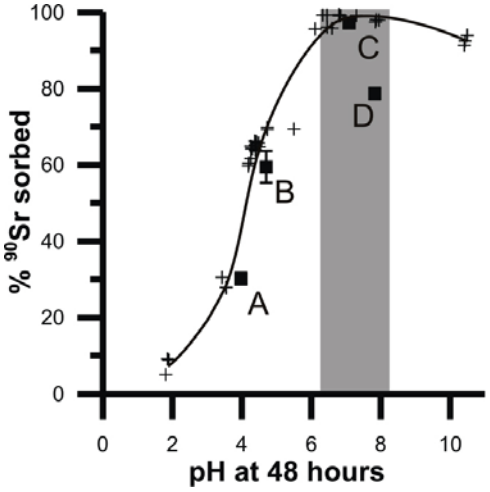

Figure 2: Effect of variation in pH on%^{90}Sr sorption. Data marked with (+) are from experiments in a sediment-water system (ionic strength = 0.05 mol /L; solid (Sr) = 1 mg/L). Also plotted % ^{90}Sr sorption for (A) Nitric acid affected groundwater, (B) Unbuffered groundwater, (C) Buffered groundwater, (D) Magnox tank liquor. Grey shaded area outlines the pH range measured at the Sellafield nuclear site

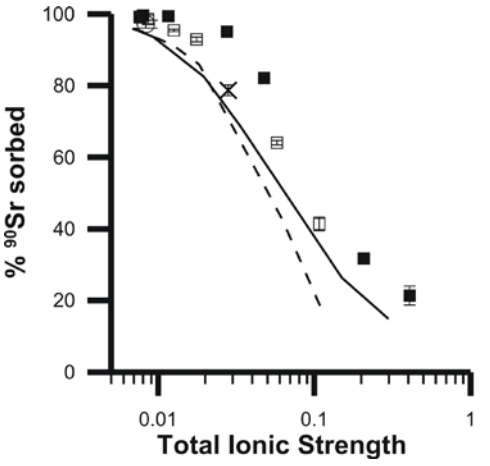

Figure 3: Effect of increasing Na^+ (□) and Ca^{2+} (■) concentration in a groundwater based sediment-water system on ^{90}Sr sorption. Also plotted % ^{90}Sr sorption after 48 hours for buffered groundwater (○) and Magnox tank liquor (X) versus their total cation concentration (ionic strength, mol/L). Solid and dashed lines represent results from PHREEQC cation exchange modelling considering the effects of Ca^{2+} and Na^+ concentrations respectively

Incorporation of ^{90}Sr in alkali altered mineral phases

Sorption of ^{90}Sr in sediments reacted with young cement water (YCW) at pH 13.5 was found to be >99 % despite the extremely high ionic strength of the solution (0.55 mol/L). At this ionic strength sorption should be inhibited by competing ions (Fig 3 above). This enhanced uptake suggests the presence of a strongly sorbing phase that is not present in unreacted sediments. In sequential extractions, it was found that ^{90}Sr was exchangeable by $MgCl_2$ at pH 7 in samples aged at room temperature, but in a sample aged for 365 days at 70 °C, ~60 % was associated with the reducible phase (extracted by 0.5 M hydroxylammonium chloride, pH 1.5, 12 hours) and ~25 % was associated with residual phases (i.e. not extracted in any of the solutions used).

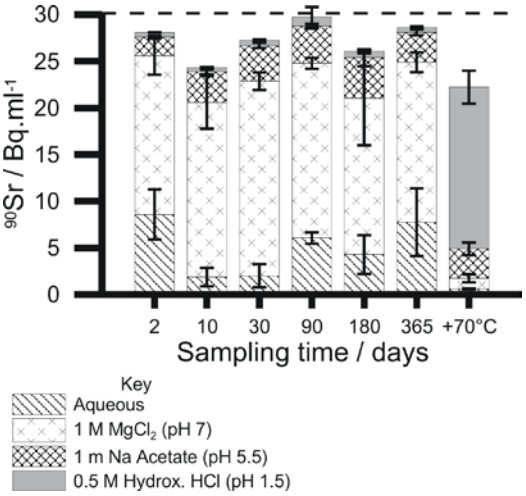

Figure 4: ^{90}Sr concentrations recovered in sequential extractions performed on sediments aged in YCW solution. Dashed line at 30 Bq ml^{-1} equates to 100% recovery

XRD results (not shown) indicated that the mineralogy of the sediments did not change during the reaction with YCW up to 365 days, however the intensity of the chlorite peaks (relative to illite/muscovite peaks) was reduced in samples reacted with YCW compared to unreacted sediments. SEM analysis of the unreacted sediment (Figure 5A) revealed sand and silt sized quartz and feldspar grains coated with <5 µm aluminosilicate clay particles with a plate-like morphology. After 10 days reaction with YCW (Figure 5B) the clay particles were still visible as a surface coating on the grains, but their surface appeared altered, i.e. smoother. EDX analyses of the aluminosilicate clay particles showed they contained elevated potassium compared to the material coating the unreacted sediments. After 365 days reaction (Figure 4C), the surfaces of the grains were coated with a smooth fine grained (i.e. nanoparticulate) secondary precipitate. For the 70 °C treated

sample SEM (Fig 5D) shows the presence of new disc-shaped (~10 µm diameter) crystal growths on the surfaces of sediment grains. XRD and electron microprobe analyses (data not shown) have confirmed these as the zeolite K-chabazite, which is known to incorporate Sr. Chabazite is unstable below pH 2, and this explains why ^{90}Sr is extractable with hydroxylamine HCl at pH 1.5. The formation of the alkali alteration products was reflected in the analysed fluid composition (not shown) by initial rapid increases in dissolved silicon and aluminium resulting from dissolution of clay minerals, followed by a slower decline as the secondary aluminosilicate gel and zeolite phase are formed.

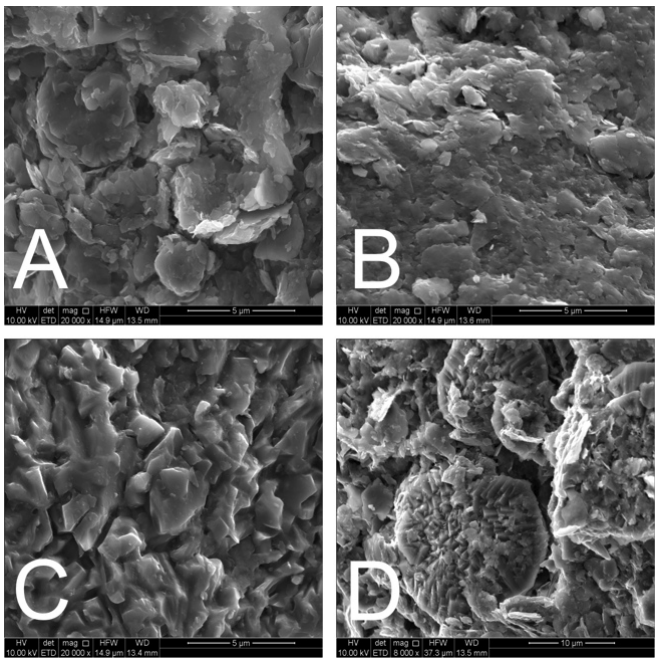

Figure 5: Scanning electron photomicrographs of sediment samples under the following conditions. A) Unreacted coarse sediment; B) after 10 day reaction in YCW; C) after 365 days reaction in YCW, and; D) after 365 days reaction at 70°C

EXAFS analyses of sediments reacted at room temperature show some evidence of Si(Al) backscatterers at 3.69 Å, 3.84 Å and 4.12 Å (Fig 6). As the ^{90}Sr in these experiments was exchangeable, we suggest that the ^{90}Sr is adsorbed as an inner-sphere complex at weathered clay edge sites. In the sample reacted for 365 days at 70 °C, a strong Sr-Si(Al) bond distance of 3.45 Å was found. These mechanisms of ^{90}Sr sorption under strongly alkaline conditions (pH 13.5) that result from interaction of YCW with sediment are therefore distinct from that observed buffered by neutral groundwater and Magnox corrosion products (pH 10-11), where an outer-sphere complex is proposed based on EXAFS.

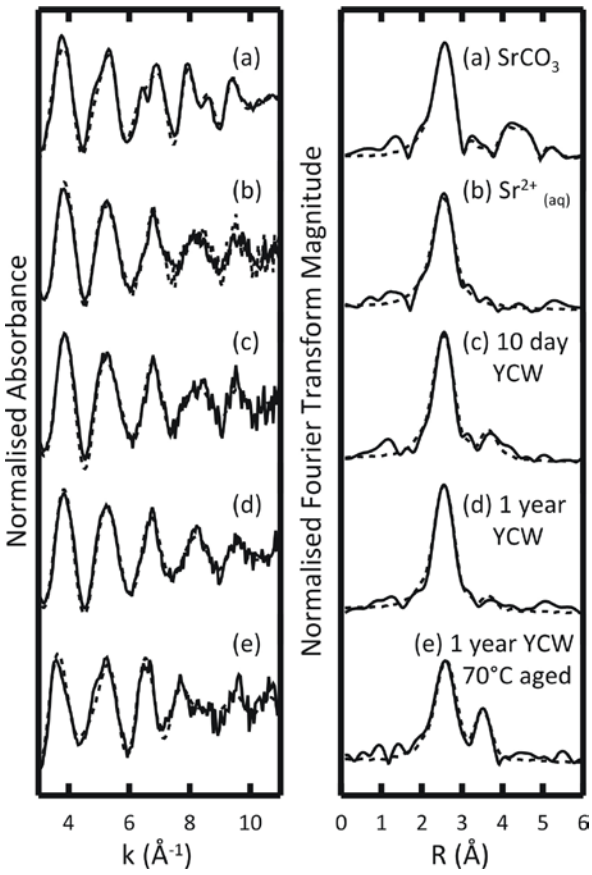

Figure 6 Background subtracted Sr K-edge EXAFS spectra (left hand side) and related Fourier transformations (right hand side) collected from a 3000 mg/L Sr^{2+} solution, $SrCO_3$ and sediment samples aged with Sr^{2+} and YCW for 10 days, 365 days, or 365 days at 70°C

CONCLUSIONS

Under the pH and salinity conditions associated with ground contamination in nuclear facilities three main mechanisms of ^{90}Sr sorption have been deduced (Fig 7), which involve the formation of outer-sphere or inner sphere ^{90}Sr complexes or the incorporation of ^{90}Sr into sites within the structure of zeolite alteration products. These mechanisms have the following implications for ^{90}Sr mobility.

- In low ionic strength groundwaters, such as at Sellafield, ^{90}Sr is least mobile at circumneutral pH. Under these conditions ^{90}Sr adsorbs strongly to sediment surfaces in outer sphere-complexes, but is exchangeable with $MgCl_2$ and is likely to be affected by subsequent increases in groundwater salinity.
- At higher ionic strengths, such as associated with Magnox liquors and in saline groundwaters, ^{90}Sr sorption is reduced due to competition by alkali and alkali earth cations and so under these conditions ^{90}Sr is potentially more mobile.

- Where alkaline cement waters are in contact with sediments mineral alteration reactions may promote the formation of inner sphere complexes with clay minerals, which enhance sorption even at high ionic strength. At elevated temperature and possibly over long timescales at ambient temperature ^{90}Sr may be inorporated into alkali alteration products which potentially make ^{90}Sr more recalcitrant to remobilisation.

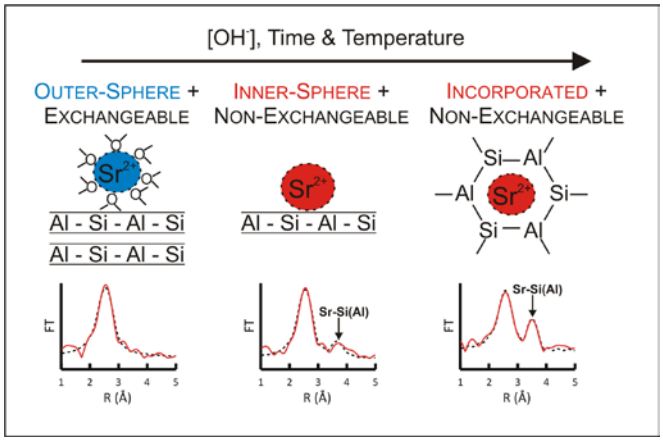

Figure 7: Schematic of the mechanism derived by EXAFS of ^{90}Sr sorption onto aluminosilcates in alkali affected contaminated ground

Acknowledgements

This research was undertaken primarily by Dr Sarah Wallace as part of her PhD at the Univeristy of Leeds, under the supervision of Dr Ian Burke. Prof. Kath Morris, Dr Sam Shaw (both now at University of Manchester) were co-supervisors of the studentship and are thanked for their guidance and scientific input. Dr James Graham (NNL) and Sellafield Ltd are thanked for the provision of generic data on Magnox sludge liquor composition. The research was funded by the UK Engineering and Physical Science Research Council and the UK Nuclear Decommissioning Authority (Award 07000878). The European Synchrotron Radiation Facility is thanked for access to beamline BM26a (Grant EC-740), and we acknowledge support from UK Natural Environment Research Council Grant NE/H007768/1.

References

1. Wallace, S.H.; Shaw, S.; Morris, K.; Small, J.S.; Fuller, A.J.; Burke, I.T., "Effect of groundwater pH and ionic strength on strontium sorption in aquifer sediments: Implications for 90Sr mobility at contaminated nuclear sites", *Applied Geochemistry*, **27**, 1482, (2012).

2. Wallace, S. H.; Shaw, S.; Morris, K.; Small, J. S.; Burke, I. T. "Alteration of Sediments by Hyperalkaline Cement Leachate: Implications for Strontium Adsorption and Incorporation", *Environ. Sci. Technol.*, **47**, 3694, (2013).

THE INHIBITION OF LOCALISED CORROSION IN IRRADIATED COOLING WATERS

Guy Whillock
guy.oh.whillock@nnl.co.uk

INTRODUCTION

Cooling water systems for nuclear waste constructed from certain austenitic stainless steel are known to be susceptible to localised corrosion. The corrodant is the chloride ion which is present in the water in a low, but significant given other factors, concentration (< 10 mg/L). Localised corrosion processes exhibit an initiation and a propagation phase, the difference between the two relating primarily to the establishment of a stable occluded cell where corrosion products are trapped and hydrolyse producing acidity, thereby altering the local solution chemistry in favour of local metal dissolution. Certain chemicals can be added to the water to inhibit (i.e. retard) localised corrosion processes and it is always the case that it is much easier to inhibit the initiation phase because the occluded cell has not developed fully. Owing to the age of the cooling system of interest by the time that the corrosion mechanism had been identified, it was clear that any corrosion sites would be fully developed. Hence, candidate corrosion inhibitors would have to be shown to be effective against propagating corrosion, requiring the development of a specific corrosion test method, as outlined in this article and related references (1-9).

Background

Stainless steels are passivated by a thin, tenacious oxide film consisting primarily of Cr_2O_3. This effectively insulates the underlying metal from contact with its environment. However, passivity can be disrupted leading either to uniform corrosion or localised corrosion depending primarily on the environment. Reducing acids such as hydrofluoric and hydrochloric acids tend to promote uniform corrosion, leading to general metal thinning. Chloride ions in near-neutral solutions, however, tend to promote localised film-breakdown; in this case, general thinning does not occur, but penetration takes place at discrete points. Localised corrosion processes fall into three broad categories, viz. crevice corrosion, pitting corrosion and stress corrosion cracking. The last of these requires the presence of tensile stresses of sufficient magnitude and is highly metal/environment specific. Common to all localised corrosion mechanisms is the establishment of an occluded cell where the local environment becomes significantly different from the bulk by virtue of spatial separation of the anodic and cathodic partial reactions (i.e. the oxidation (metal dissolution) and reduction (e.g. of dissolved oxygen) reactions respectively) that constitute the corrosion process (Equations 1a and 1b). Local metal dissolution supported by a remote cathode creates a charge imbalance which is negated by the migration of anions to the former (and cations to the latter). Chloride ions, being generally present and highly mobile by virtue of their small size and high charge density, migrate to the active corrosion site (Equation 1c), but the corrosion products so formed hydrolyse reducing the pH (Equation 1d):

$$4Cr \rightarrow 4Cr^{3+} + 12e^- \quad (1a)$$

$$3O_2 + 6H_2O + 12e^- \rightarrow 12OH^- \quad (1b)$$

$$Cr^{3+} + 3Cl^- \rightarrow CrCl_3 \quad (1c)$$

$$CrCl_3 + (3-x)H_2O \rightarrow Cr(OH)_{3-x}Cl_x + (3-x)H^+ + (3-x)Cl^- \quad (1d)$$

where x is 0, 1 or 2 (Equation 1d). Iron and nickel chlorides also hydrolyse, but do not reduce the pH to the same extent as chromium.

Since stainless steels are corroded by hydrochloric acid, the process is autocatalytic, leading to the development of a local environment where the pH is typically < 2 and the chloride ion concentration may be several mol/L whilst the bulk environment remains essentially neutral and of very low chloride ion concentration. The vast majority of the metal surface remains passive and is quite unattacked, but actively corroding sites can be deeply penetrated, leading to perforations.

For the cooling water system of interest, the chloride ion concentration is very low (< 10 mg/L) and would not normally be sufficient to promote corrosion of 18% Cr stainless steels. However, the

water is used to cool radioactive wastes and hence is radiolysed in situ, producing hydrogen peroxide in concentrations ranging between ~ 0.5 and ~ 5 mg/L depending on the radiation dose received (which is a function of the isotopic content of the waste and the residence time in the radiation field). Hydrogen peroxide is a more powerful oxidant than dissolved oxygen and stimulates the anodic metal dissolution reaction. An extensive programme of radiation testing, backed up by tests employing hydrogen peroxide to simulate the bulk effect of water radiolysis, showed that the initiation of crevice, but not pitting corrosion, was possible and in fact occurred readily even at representatively low chloride ion concentrations. The difference between the two mechanisms relates primarily to the presence or absence of a geometric inhomogeneity (a defect) that facilitates the entrapment of corrosion products, hence favouring development of an occluded cell. Defects of various degrees of severity are present in any structure as a consequence of its manufacture and range between unavoidable crevices formed as a result of certain weld procedures and inadvertent, undetected defects such as minor rolling laps, scratches or minor weld bead porosity etc. The defects play a crucial role since they allow corrosion to initiate in conditions that would otherwise be too benign. Figure 1 shows an example of crevice corrosion, marked by the rusty patches, that occurred when a pipe that had been scored by a mandrel when it was bent was corrosion tested under representative conditions. Had it not been for the scores, no corrosion would have occurred.

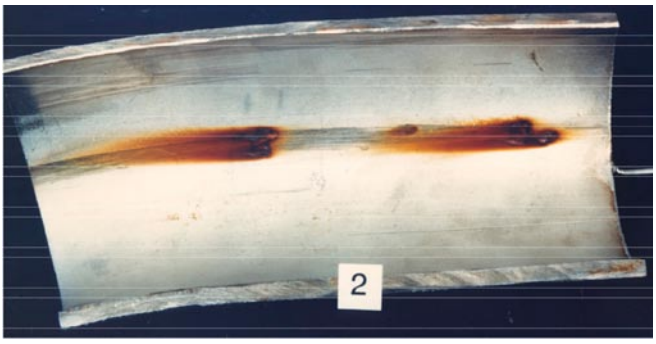

Figure 1: Appearance of a NAG 18/10L pipe (80 mm ID) after corrosion testing (10 mg/L Cl^-, 600 Gy/h, 25 °C)

Although the corrosion process initiates solely at crevices in this case owing to the marginal environmental conditions, propagation results in the formation of cavities in the metal that are filled with the corrosive, occluded liquor. Such cavities are electrolytically connected to the external environment by a small entrance hole or series of holes that prevent washing out of the occluded liquor. Figure 2 shows an example of a corrosion site found in a man-accessible part of the cooling water system (downstream of the radiation field, hence the water contained hydrogen peroxide). A cavity with approximate dimensions of 28 x 10 x 4 mm3 had formed despite the fact that the plate was only 4.7 mm thick i.e. the interior of the plate had been dissolved, bounded by thin metal ligaments. The initiating crevice was a scratch-like defect that was shown by sectioning to be consistent with a rolling lap. Propagation led to the formation of a large pit cavity aligned with the direction of gravity and the rolling direction of the plate; the "tail" at the bottom of the pit (see Figure 2a) delineates an inclusion stringer that had been dissolved ahead of the main corrosion front. Numerous other examples have been found in accessible parts of the cooling water system, confirming that the mechanism produces large pit cavities within relatively short timescales. Hence, the challenge was to develop an inhibition treatment that would be effective against large, mature pits rather than crevices per se, necessitating the development of a corrosion test method for this specific application.

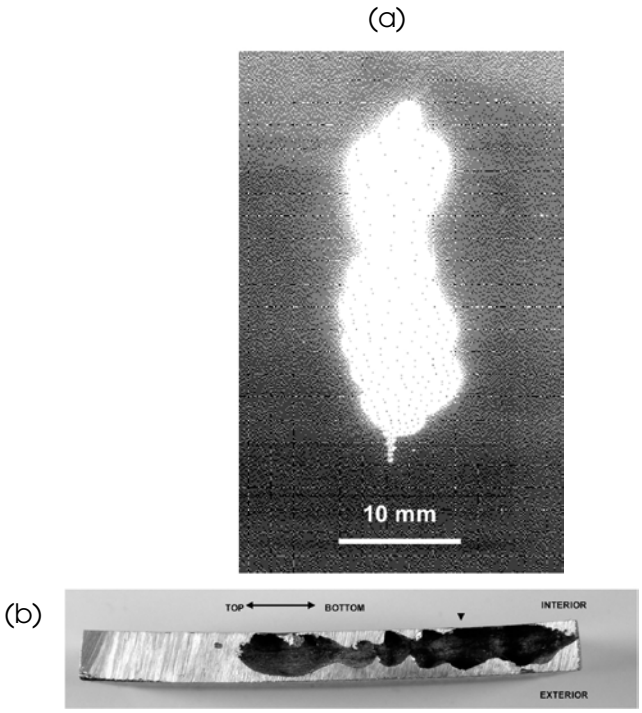

Figure 2: Cavity formed in a 4.7 mm thick plate after 12 year's exposure to irradiated cooling water: (a) radiograph taken face-on; (b) cross-section

Artificial corrosion pits

At the outset, it was decided to mimic the features observed in the real pits that had been examined previously, viz. approximately the same pit cavity volume to area ratio, numerous small entrance holes, pit solution containing Fe, Cr and Ni in stoichiometric proportion to the composition of

the stainless steel used in plant construction, pit encased in ferruginous sludge.[1] In addition, the ability to differentiate between corrosion occurring due to external and internal cathodes was considered necessary (since this would inform as to the action/fate of candidate inhibitors), as was the ability to determine composition changes within the pit solution as testing progressed.

The design depicted in Figure 3 was found to be workable. It consisted of a stainless steel wire dipped into a plastic bulb that was filled with pit solution consisting of iron, chromium and nickel chlorides. The plastic bulb contained a number of fine (0.5 mm diameter) holes that provided electrolytic connection to the bulk environment and also served to vent hydrogen gas that could be produced within the pit cell under some circumstances. The pit cell was surrounded by a stainless steel mesh cylinder, the two being electrically connected by a zero resistance ammeter (ZRA). The wire electrode formed the working electrode (WE) and the mesh formed the auxiliary electrode (AE). The total corrosion rate was determined from the weight loss of the WE and the external contribution was obtained by application of Faraday's law to the charge passed. The difference between the two provided the contribution to the corrosion process made by any cathodes acting internally to the pit cell.

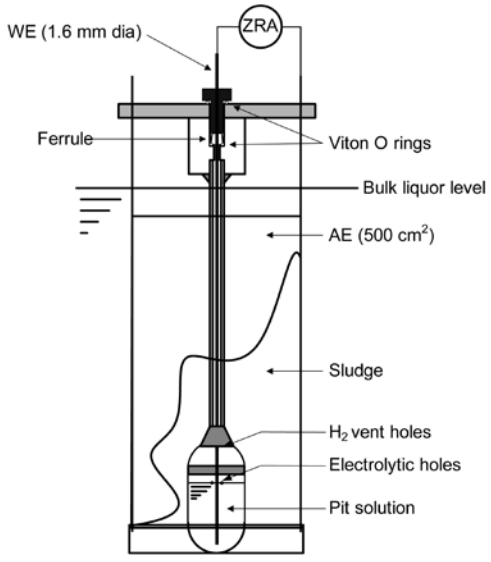

Figure 3: Cut-away sketch of the wire-electrode artificial pit (not to scale)

This design of pit cell was used to investigate various factors such as the effect of varying the number of electrolytic holes, the effect of different configurations of ferruginous sludge, and the effect of varying the strength of the pit solution. On the basis of those trials, the most viable set-up was selected and shown to be capable of exhibiting stable corrosion at high corrosion rates for long periods, this being a pre-requisite for testing of inhibitors. Figure 4 shows some results obtained, indicating that the pit solution pH tended towards a value of ~ 2 and its chloride concentration tended towards ~ 10 g/L with almost all the corrosion process being driven by the external cathode.

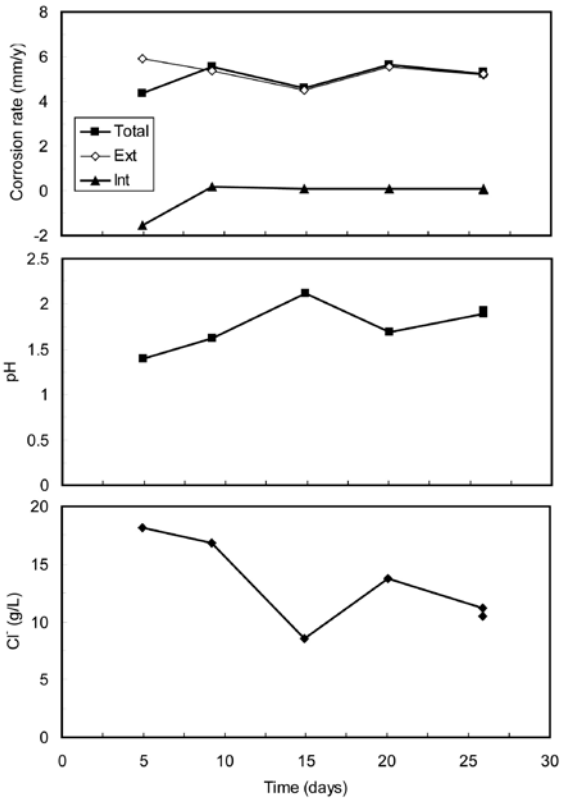

Figure 4: Wire-electrode test results: 304L stainless steel WE (1.6 mm diameter); 1.5 mol/L $FeCl_2.4H_2O$, 0.42 mol/L $CrCl_3.6H_2O$, 0.27mol/L $NiCl_2.6H_2O$ pit solution; natural water/15 mg/L Cl^- + 5 mg/L H_2O_2 bulk solution; 60 °C

However, whilst the design of the wire-electrode pit was successful, it was adapted to remove its polymeric constituents since it was anticipated that direct radiation testing would be required, resulting in an all-metal artificial pit. The ensuing corrosion tended to proceed downwards from the cavity, as exhibited by Figure 5. The internal morphology of the corroded artificial pit cavities, although not shown here for brevity of presentation, was similar to that revealed by destructive examination of the pit shown in Figure 2 and other examples obtained from the cooling water system.

1 *Although constructed from stainless steel, the cooling water system of interest is supplied by water fed via a cast iron pipe. Over the years, considerable quantities of iron oxide corrosion products, derived form the cast iron, accumulated in some parts of the cooling system.*

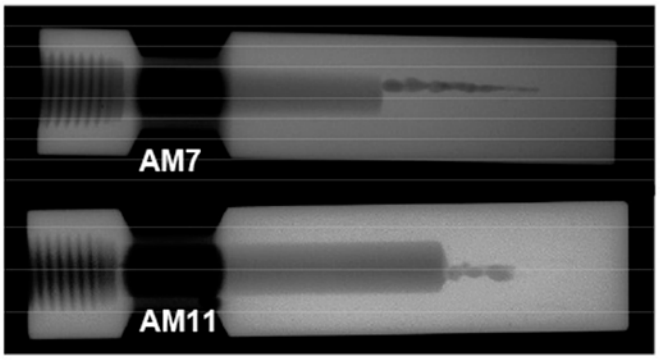

Figure 5: Radiograph of two different all-metal artificial pit specimens showing secondary pits that had emanated from the bases of the internal cavities (5 mm drilled hole). Each specimen's external length is 55 mm. The specimens were oriented vertically during testing with the threaded ends uppermost

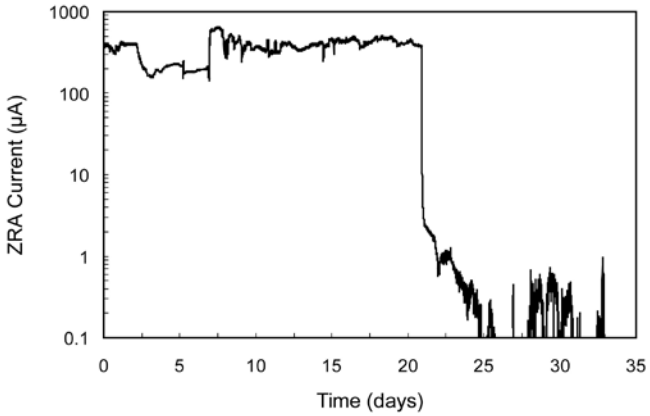

Figure 6: Inhibition by nitrate: wire-electrode artificial pit, filled with 0.6M Fe(II) solution, tested at 60 °C in natural water dosed to 15 mol/L Cl^- , 15 mg/L hydrogen peroxide and 3,000 mg/L nitrate

Inhibitor trials

A number of candidate inhibition treatments were selected for trial on the basis that they were already known to be effective for some forms of localised corrosion and would be suitable for deployment. Demineralised water (i.e. removing the corrodant chloride ion), sodium hydroxide, sodium molybdate and sodium nitrate were tested. Of these, only sodium nitrate was found to be effective, noting that hydroxide and molybdate might well have been more effective if their dosage had been increased (but that would have prevented plant deployment). Demineralised water was found to be of uncertain effect since the very low conductivity prevented meaningful ZRA measurements and some specimens indicated almost immediate current increase $^{-1}$ when the bulk water was switched back to 15 mg/L chloride (following soaking in demineralised water for > 200 days previously), indicating, rather surprisingly, that complete removal of the occluded pit solution could not have occurred.

Figure 6 shows that inhibition by nitrate took a few weeks to take effect, but when it occurred it was sudden, the corrosion process ceasing within a few minutes only. This appears to indicate the achievement of a critical pit solution chemistry, which rapidly switches the metal from active to passive corrosion states when the pit solution switches from being predominantly hydrochloric acid to predominantly nitric acid. The latter passivates stainless steel, whereas the former actively corrodes it. Since a reasonably long time was invariably required for inhibition by nitrate to take place and nitrate/chloride mixtures are known to support active/passive transitions, concern was raised that nitrate treatment might switch the corrosion process from essentially general corrosion within the pit cavity to stress corrosion cracking (SCC).

Stressed artificial pit

In order to investigate a plausible switch to SCC, the most expedient way forward was to adapt the design of the all-metal pit to introduce tensile stresses at the base of the pit cavity. This was done by incorporating a notch in the base of the specimen, thus forming a pair of legs that could be loaded either in tension or compression to create a stress field ahead of the notch. Figure 7, which is a radiograph, illustrates the principle by which a bolt can be used to load the specimen compressively, generating a compressive stress field immediately ahead of the notch balanced by a tensile stress field further away from the notch.

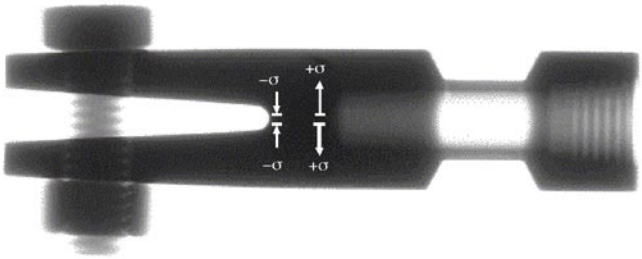

Figure 7: Radiograph showing the principle of specimen loading to produce tensile stress in the base region of the pit cavity

To validate the design, surface strain measurements were made on a small number of non-corroding, loaded specimens using electron speckle pattern interferometry. Tests were carried out to inform as to whether compressive or tensile loading of the bolt was more advantageous, how much load should be applied and whether a long or short notch should be preferred. The results indicated that tensile loading of the specimen did not generate a tensile stress field for a pit to grow into, except very near to the notch tip. Compressive loading was better because it provided a region of tensile strain over a distance of several mm at a position

ahead of the notch and in particular, nearer to the base of the cavity. The surface strain measurements implied that for the notch to create a tensile stress field of the order of the proof strength, in the metal ahead of a downward-propagating pit, the pit should be at a distance of about 1 to 3 mm from the notch for the selected leg displacement (1 mm at the point of bolt loading). Tests were then carried out in environments that were conducive to SCC using 304 grade stainless steel specimens that had been sensitised[2] to confirm that the stressed pit was indeed capable of exhibiting SCC. Figure 8 shows that cracking was indeed induced at the base of the cavity as intended.

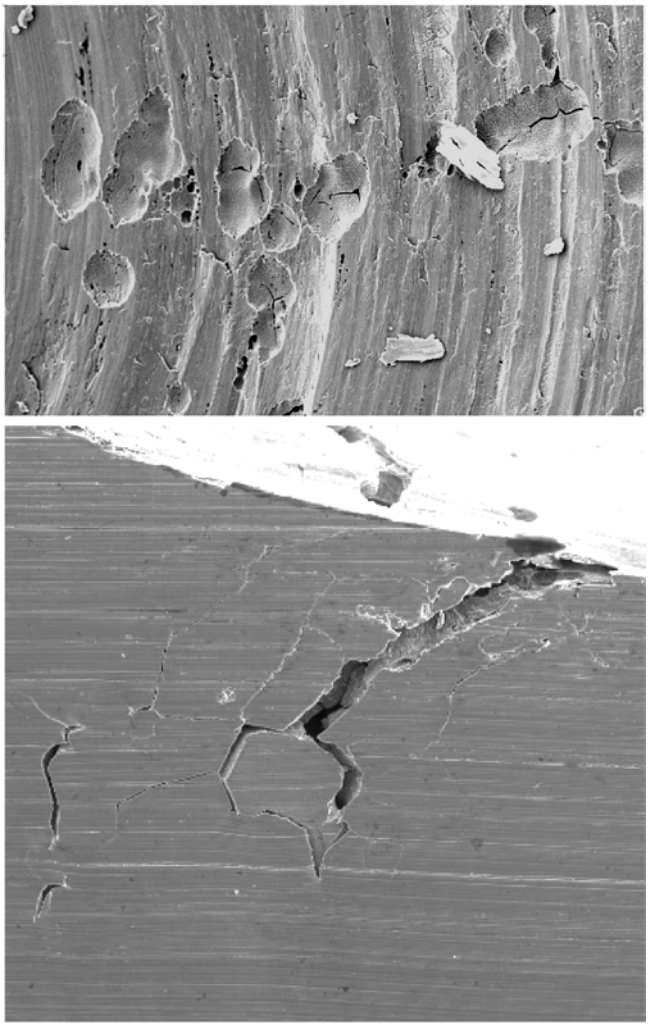

Figure 8: Stress corrosion cracks produced in stressed all-metal pit fabricated from sensitised 304 stainless steel; (a) view looking down on the base of the pit cavity; (b) cross-section of a crack initiated from the pit cavity (mechanically opened post-test to aid viewing)

Radiation tests

Two campaigns of radiation tests were carried out in a ^{60}Co cell to confirm the efficacy of nitrate dosed at 50 g/l, which by then had been established as likely to be sufficient (but not overly so). The stressed variant of the artificial pit was used and these were made from three materials: 18/13/1, the steel used in the cooling water system; S34780 weld metal (i.e. specimens were cut from a suitably large double-vee weld made for this purpose), and; 304 grade stainless steel that was thermally sensitised to induce greater SCC susceptibility. Testing was carried out at two temperatures, 60 and 90 °C, the former being typical of plant conditions, the other representing a fault condition that would also engender increased susceptibility to SCC should the conditions within the pit be thus conducive. The radiation dose rate received by the water in each test vessel (see Figure 9) was ~ 500 Gy/hr, resulting in a hydrogen peroxide concentration in the bulk water of 2 mg/L (i.e. representative of plant conditions).

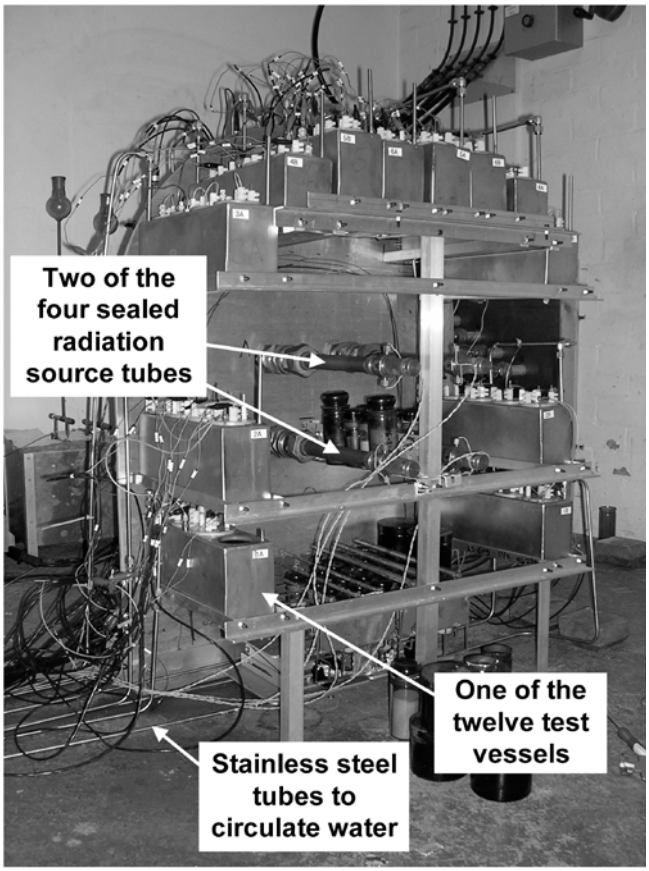

Figure 9: The experimental setup in the radiation cell. The experiment was mounted on an aluminium backing plate so that that test vessels would be approximately equidistant from the ^{60}Co radiation sources

2 *Certain heat treatments, notably encountered during welding, promote the formation of chromium carbides, resulting in chromium depletion in a narrow band adjacent to grain boundaries. This is termed sensitisation.*

Figure 10 shows results obtained for the weld metal at 60 °C, which are typical of all results. The control sets, which were not dosed with nitrate exhibited ZRA currents indicative of corrosion for the duration of testing, although a small number of specimens corroded only weakly. For the sets that were treated with nitrate, noting that this was introduced following a long period (> 40 days) of prior corrosion in an effort to establish steady state conditions within the artificial pits, nitrate dosing promoted a marked, but short-term increase in current, followed by a fall to very low and negative currents. The negative current indicates a switch from anodic to cathodic behaviour relative to the external stainless steel mesh, most likely due to the appearance of nitric (or nitrous, since it is irradiated) acid within the pit solution.

Destructive examination of the 18/13/1 and weld metal specimens indicated no SCC. However, the sensitised 304 specimens were found to have suffered extensive SCC, but this was common to both control and nitrate-treated sets. This result merely indicates the importance of the material; under these conditions, thermally sensitised 304 grade stainless would exhibit a transition from crevice corrosion to SCC, whereas for 18/13/1 a transition from crevicing to pitting is favoured.

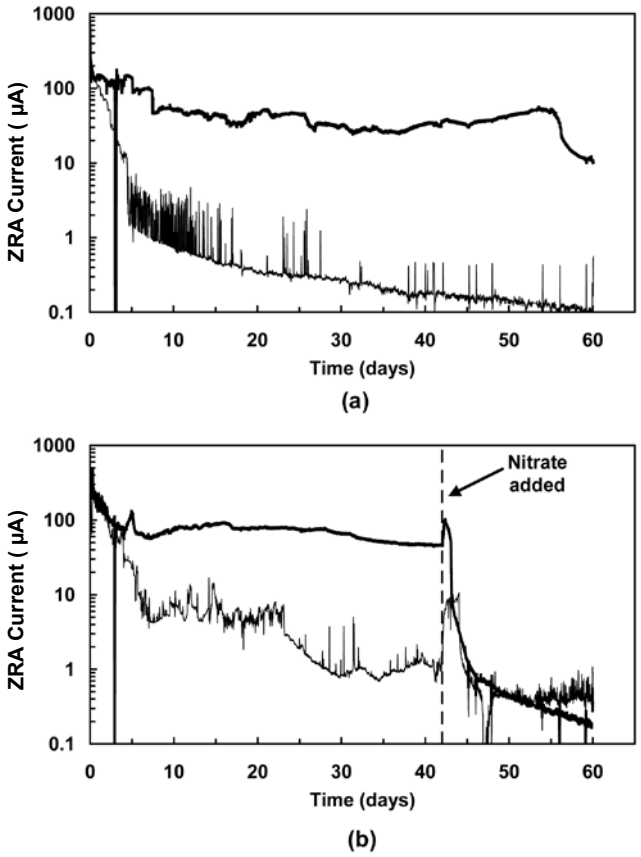

Figure 10: The effect of 50 g/L nitrate at 60 °C on irradiated stressed all-metal artificial pits made from S34780 weld: (a) a control test that was not nitrate-dosed, and (b) a test that was subjected to nitrate dosing. For clarity, each graph only shows two results which are chosen to bound the behaviour of all the specimens

CONCLUSION

Whilst nitrate dosed to a bulk solution concentration of 50 g/L effected full passivation in all cases, the short-term increase in ZRA current promoted by nitrate addition warrants consideration (see Figure 10). The simplest, and arguably safest, interpretation to place on this observation is that nitrate temporarily increases the corrosion rate of the pits prior to inhibition's taking hold. The increase in current flow must, initially at least, be due to the increased conductivity (i.e. augmentation of the cathode) rather than increase in the anodic dissolution reaction, although nitrate is known to affect this, since the effect is essentially instantaneous. Later on, augmentation of the anodic dissolution reaction might occur depending on the changing pit solution composition.

Although the increase in current promoted by nitrate was always temporary, this result applies only to the pit geometry tested. It was considered plausible that deeper pits might extend the duration of corrosion acceleration by nitrate. A small number of scoping experiments generally supported that supposition. In addition, a concern existed over whether nitrate treatment could promote a change from microstructurally-sensitive (i.e. predominantly following the hot-working direction of the metal) to microstructurally-insensitive growth, thus potentially posing issues for the through-wall penetration rate. Accordingly, it was decided that nitrate inhibition (this being the only treatment that had been found actually to be effective) was potentially unsafe. Further work would be required to develop unequivocal techniques for measuring the effect of nitrate on the corrosion rate, there being uncertainty attached to interpretation of the ZRA current data. X-ray tomography methods were identified as offering the potential to resolve metal dissolution directly in real time, these having the advantage of being able to detect, in principle at least, any change in the preferential growth direction. Scoping tests that showed some promise were carried out. However, it was decided that the outcome of further work was too uncertain and the timescales were too long. Hence, effort to develop a corrosion inhibitor for this application was abandoned.

Acknowledgements

The contributions to this research made by Sam Worthington, Tracey Binks, Pete Apps and Neil Donohoe are acknowledged. The author is indebted to Sellafield Ltd and its precursor, BNFL, for financial support and to specific individuals in those organisations for sponsoring long-term research in this area.

References

1. R C Newman: "Understanding the corrosion of stainless steel", *Corrosion*, **57**, 1030, (2001).

2. G O H Whillock: "Corrosion in radiolysis induced environments" in "Shreir's Corrosion" (J A Richardson et al eds.), Vol. 2, 1330 – 1339, Elsevier, Amsterdam (2010).

3. G O H Whillock, S E Worthington, and C J Donohoe: "Localized corrosion of stainless steel in a nuclear waste cooling water system — Part 1: Crevice corrosion studies" *Corrosion*, **68**, 677, (2012).

4. C J Donohoe, G O H Whillock, and P J Apps: "Localized corrosion of stainless steel in a nuclear waste cooling water system — Part 2: Plant inspection findings", *Corrosion*, **68**, 844, (2012).

5. G O H Whillock, T J Binks, and C J Donohoe: "Localized corrosion of stainless steel in a nuclear waste cooling water system — Part 3: Development of a large artificial pit", *Corrosion*, **68**, 859, (2012).

6. G O H Whillock, T J Binks, and C J Donohoe: "Localized corrosion of stainless steel in a nuclear waste cooling water system — Part 4: Artificial pit investigation of nitrate inhibition", *Corrosion*, **68**, 967, (2012).

7. C J Donohoe and G O H Whillock: "Localized corrosion of stainless steel in a nuclear waste cooling water system — Part 5: Inhibition studies using "all-metal" artificial pits", *Corrosion*, **68**, 1076, (2012).

8. G O H Whillock and C J Donohoe: "Localized corrosion of stainless steel in a nuclear waste cooling water system — Part 6: Testing for stress corrosion cracking susceptibility", *Corrosion*, **69**, 9, (2013).

9. C J Donohoe and G O H Whillock: "Localized corrosion of stainless steel in a nuclear waste cooling water system — Part 7: Direct radiation experiments", *Corrosion*, **69**, 107, (2013).

NEWS STORIES

NEW POSITION PAPER – MINOR ACTINIDE TRANSMUTATION

NNL has many years experience of the nuclear fuel cycle and associated science and technology and is in an ideal position to advise decision makers on key topics which are important when considering the UK's ability to meet these nuclear challenges. NNL's view on these topics is being set out as a series of Position Papers. These papers reflect our independent and authoritative view and are supported by underpinning studies.

A new position paper has recently been published on Minor Actinides Transmutation. For many years there has been a sustained international interest in partitioning and transmutation of the minor actinides neptunium, americium and curium produced by fission reactors. Although these three elements are produced in relatively small quantities, they are major contributors to the decay heat, neutron output and radiotoxicity of spent nuclear fuel. Implementation of minor actinide transmutation on a commercial scale will require major research and development effort sustained over many years and is not likely to be available for at least twenty years. This position paper sets out the view of the UK National Nuclear Laboratory (NNL) of the potential role of minor actinide transmutation in the context of nuclear waste management in the UK.

Other position papers include:

- Boiling Water Reactors Position Paper
- Proliferation Resistance and Physical Protection Position Paper
- Fuel Cycle R&D to Safeguard Advanced Ceramic Fuel Skills
- Thorium
- Small Modular Reactors

Copies of the position papers can be downloaded from the webpage below:
http://nnl.co.uk/science-technology/position-papers.aspx

DISTINCTIVE

EPSRC has approved a £6,126k (full economic cost) collaborative research programme in Decommissioning, Immobilisation and Management of Nuclear Waste, to be carried out by the DISTINCTIVE* consortium of 10 universities led by Prof Simon Biggs at Leeds. The programme, which will begin in February 2014 and run for 4 years, comprises 30 projects within four themes, (i) AGR, Magnox and Exotic Spent Fuel, (ii) PuO_2 and Fuel Residues, (iii) Legacy Ponds and Silos Wastes and (iv) Structural Integrity. The programme includes substantial contribution from NNL, NDA and SL, bringing the total programme value to £8,122k. The NNL is providing a large contribution including teaching, industrial supervision of about half the projects, the allocation of two CASE awards as well as facility costs at Central Laboratory for around five students and postdoctoral researchers. The secondments include two long term (2 year) PDRA placements from the Universities of Manchester and Lancaster, who will work on the behaviour of PuO_2 during interim storage.

** DISTINCTIVE = Decommissioning, Immobilisation and Storage soluTIons for NuClear wasTe InVEntories. The full list of partner universities is Universities of Manchester, Sheffield, Lancaster, Birmingham, Strathclyde, Leeds, Loughborough, Bristol, Imperial College and UCL.*

COLLABORATION BETWEEN RADIATION CHEMISTS AT NNL AND ATOMIC ENERGY OF CANADA LTD (AECL)

Members of NNL's Radiation Chemistry and Modelling team, based at Harwell and Stonehouse, are collaborating with radiation chemists at AECL's Chalk River Laboratory on an experimental and modelling study of nitric acid formation in carbon dioxide gas containing traces of air.

The National Research Universal (NRU) reactor at Chalk River, which is used for research and medical isotope production, had to be shut down in 2009 to repair a minor heavy-water leak from the reactor vessel. Examination of the leak site showed that the vessel wall had become corroded from the outside, where it is surrounded by a gas-filled annulus. The corrosion is thought to have been caused by nitric acid which is formed by reactions that occur in moist air in the presence of a radiation field. Although the reactor annulus is filled with dry carbon dioxide (CO_2), small amounts of air and water do leak in and these are the probable source of the nitric acid. One possible solution to this problem would be to introduce small amounts of other gases such as hydrogen (H_2) or methane (CH_4) which could change the gas chemistry and reduce or prevent the formation of nitric acid. AECL are planning a series of small-scale experiments to study the effects of these additives on the amount of nitric acid formed when representative gas mixtures are irradiated.

NNL staff in RCM have been involved for many years in developing and applying a model of the coolant chemistry in Advance Gas Reactors (AGRs). AGR coolant consists mainly of CO_2, with small amounts of other components (carbon monoxide, water vapour, hydrogen and methane). The coolant can also contain small amounts of air, and we have recently done work for EDF Energy to include the radiation chemistry of nitrogen. As a result, we now have a model that can be used to simulate AECL's proposed experiments, to help with their planning and give an indication of the expected results, In return, we will be able to use their results to assess how good our model is, and make improvements if necessary.

WINNING POSTER AT NI CONGRESS

The inaugural Nuclear Institute (NI) Congress was held in Manchester back in September. The Congress is viewed as a flagship event that brings together leaders from across the industry to address all aspects of the Government's Nuclear Industrial Strategy.
Harwell based Materials Research Scientist Dr Paul Styman celebrated success at the event when he won the NI Young Generation Network (YGN) Best Poster Award. Paul alongside NNL Chief Technologist Dr Jonathan Hyde and Professor George Smith from the University of Oxford presented their poster 'Nano-scale Characterisation of Nuclear Materials Using Atom Probe Tomography' which focused on Reactor Pressure Vessel (RPV) Embrittlement.

NICK SMITH - ROYAL SOCIETY FELLOWSHIP AWARD

National Nuclear Laboratory (NNL) Research Fellow Dr Nick Smith has been awarded a prestigious four-year Industry Fellowship by the Royal Society. Fellowships are awarded to scientists for work on a collaborative project with an academic organisation. Nick's Fellowship is hosted by The University of Manchester and will fund 50% of his research time.
Nick's primary focus is fundamental and applied research into remote 2D and 3D, laser-based characterisation techniques in the nuclear industry. This research has already seen close collaboration between NNL and The University of Manchester's School of Earth, Atmospheric and Environmental Sciences and the Laser Processing Group. Future research will also involve work at NNL's Workington Laboratory and the Dalton Cumbrian Facility (DCF). The research has significant potential in helping to solve key characterisation challenges faced by the nuclear industry.

A Chartered Geologist and Fellow of the Geological Society, Nick is NNL's lead geologist and 3D geoscientific and remote sensing/characterisation expert. He holds visiting research/teaching roles at three UK universities and holds membership of the European Federation of Geologists and the European Geosciences Union

AUTHORS' BIOGRAPHIES

Nick Gribble - Nick is an internationally recognised specialist in nuclear waste immobilisation with more than 25 years experience and knowledge of vitrification processes both in the UK and abroad. He is the recognised expert on the process equipment and its operation at the Waste Vitrification Plant (WVP) at Sellafield. He is the Technical Lead for the High Temperature Waste Immobilisation section of NNL responsible for the content and quality of the work performed in support of WVP. Nick, a chemical engineer, was instrumental in the design and construction of the full scale replica Vitrification Test Rig (VTR) and is heavily involved in its programme of work, its analysis and application on WVP. He is a member of the Highly Active Waste Technical Committee and the technical authority on the Product Quality Review Committee for WVP.

Rick Short - Prior to joining NNL, I studied for a PhD at the Immobilisation Science Laboratory at the University of Sheffield, a University Research Alliance lab set up originally with BNFL funding. After becoming the first student to graduate from the ISL, I took up a position as a materials scientist within NNL and have been working with the Vitrification Test Rig team for the last 8 years. I also work closely with our primary customers, the Sellafield Ltd Waste Vitrification Plants, as well as supervising several current PhD students carrying out projects related to high level waste vitrification.

Barbara Dunnett (BSc, CChem, MRSC) has a 1st class BSc (Hons) in chemistry, awarded by the University of Glasgow. She has worked at NNL/BNFL for almost 20 years after joining as a graduate trainee where she was involved in corrosion, in particular assessing corrosion of stainless steels in nitric acid environments. In 2003, Barbara moved to the vitrification team where she carried out research work packages to support the Waste Vitrification Plant (WVP). The work included assessing the product quality of glasses manufactured and the development of new glass formulations. Barbara became a Technology Manager in 2012, in the Waste Behaviour and Materials team. She is currently involved with the chemistry of the Highly Active Liquors processed through the Highly Active Evaporation and Storage (HALES) plant at Sellafield, including the Post Operational Clean Out of the solids remaining in the plant at the end of its operational life.

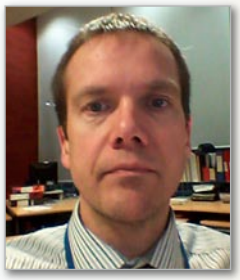

Mike Harrison (MA, DPhil, CChem) is an experienced glass chemist with over 11 years experience in the vitrification of a wide range of radioactive waste streams, including HLW, ILW, plutonium and uranium. Mike is technical lead of vitrified wasteform performance activities, and is currently directing research programmes on glass durability and leach testing. He is also providing technical expertise to both Sellafield Ltd and NDA-RWMD in order to support the disposability of UK vitrified HLW. Mike is also an expert in the treatment of molten salts waste, and is work package leader in the EU Framework VI "SACSESS" project.

Ewan Maddrell (PhD, MIMMM, CEng) is a technical specialist in ceramic and glass ceramic wasteforms based at NNL's Workington Lab. Ewan joined BNFL in 1993 and started developing wasteforms for a wide range of applications including the immobilisation of HLW from Advanced Reprocessing technologies and novel fuels, and the immobilisation of wastes and effluents which cannot be treated by existing technologies. Current research is focussed on the immobilisation of various plutonium bearing residues in durable, proliferation resistant wasteforms fabricated by hot isostatic pressing; and the application of HIP to a wider range of wastes.

AUTHORS' BIOGRAPHIES

Joe Small is the National Nuclear Laboratory's Senior Fellow for Waste and Environmental Geochemistry. He has an experimental and modelling post doctoral research background in clay mineralogy and geochemistry applied to petroleum exploration. On joining the nuclear industry in 1996 Joe has developed his modelling interests in radionuclide behaviour applied to waste disposal and contaminated land, including the evolution of wasteforms and the role played by microbiological processes. He has authored safety case documents for surface and geological disposal of radioactive waste in the UK and has research collaborations with overseas waste management organisations and research institutes. Currently, in collaboration with the University of Manchester and other UK research groups he leads a modelling workpackage in the NERC BIGRAD consortium grant that investigates biogeochemistry and radionuclide behaviour related to geological disposal.

Ian Burke is an Associate Professor of environmental geochemistry at the University of Leeds, where he is part of the Cohen Geochemistry Group in the School of Earth and Environment. His primary research interests are focused on the environmental behaviour of radionuclides and contaminant metals during nuclear decommissioning and waste disposal, in particular in understanding the processes that control trace metal speciation and mobility in soil-water systems. He has expertise in using experimental approaches to examine contaminant behaviour in natural systems; the potential for application of in situ remediation techniques; and, in the use of advanced synchrotron and electron microscope techniques for hard to characterise samples (e.g. redox active, unconsolidated and radioactive materials). His research group's on-going work is currently investigating the biogeochemistry and sorption behaviour of several priority radionuclides (^{14}C, ^{137}Cs, ^{90}Sr and ^{99}Tc) in contaminated ground at nuclear sites.

Sarah Wallace is an environmental radiochemist and obtained her PhD in 2012 from the University of Leeds. Her PhD project investigated the behaviour of strontium 90 in contaminated land scenarios relavent to UK nuclear facilities. The research focussed on the geochemical processes that control migration of strontium 90 in the sub-surface, and the effects of pH, ionic strength and groundwater composition on these processes. The aim of the project was to aid future decommissioning and remediation of legacy nuclear sites, and Sarah has had research articles published in the Journal of Applied Geochemistry and Environmental Science and Technology. Sarah has recently joined the Environment Agency, working in radioactive substances regulation.

Guy Whillock read Natural Sciences at St John's College, University of Cambridge, and then gained a PhD in corrosion science from the Department of Metallurgy and Materials Science, University of Cambridge. He joined BNFL in 1987, pursuing a career in the Materials Group of the Research and Development Department at Sellafield and its successor organisations, specialising in corrosion science. His principal interests lie in the effects of radiation on corrosion processes, primarily for stainless steels in both neutral environments containing chloride ions and nitric acid solutions, corrosion testing development, and plant life prediction and extension. He is the NNL Senior Fellow in corrosion.

(1) J. Brown; F. McLachlan; M. Sarsfield; R. Taylor; G. Modolo; A. Wilden, "Plutonium Loading of Prospective Grouped Actinide Extraction (GANEX) Solvent Systems Based on Diglycolamide Extractants" *Solvent Extraction and Ion Exchange,* **30**, 127, (2012).

(2) M. Dawson; D. Borman; R.B. Hammond; D. Lesnic; D. Rhodes, "Detection of a two-dimensional moving cavity" *International Journal of Computer Mathematics,* **89**, 1569, (2012).

(3) C.J. Donohoe; G.O.H. Whillock, "Localized Corrosion of Stainless Steel in a Nuclear Waste Cooling Water System-Part 5: Inhibition Studies Using "All-Metal" Artificial Pits" *Corrosion,* **68**, 1076, (2012).

(4) C.J. Donohoe; G.O.H. Whillock; P.J. Apps, "Localized Corrosion of Stainless Steel in a Nuclear Waste Cooling Water System-Part 2: Plant Inspection Findings" *Corrosion,* **68**, 844, (2012).

(5) B.F. Dunnett; N.R. Gribble; R. Short; E. Turner; C.J. Steele; A.D. Riley, "Vitrification of high molybdenum waste" *Glass Technology-European Journal of Glass Science and Technology Part A,* **53**, 166, (2012).

(6) E.B. Farfan; J.R. Coleman; S. Stanley; J. Adamovics; M. Oldham; A. Thomas, "Submerged Radball(TM) Deployments in Hanford Site Hot Cells Containing (CsCl)-Cs-137 Capsules" *Health Physics,* **103**, 100, (2012).

(7) E.B. Farfan; S. Stanley; C. Holmes; K. Lennox; M. Oldham; C. Clift; A. Thomas; J. Adamovics, "Locating Radiation Hazards and Sources Within Contaminated Areas by Implementing a Reverse Ray Tracing Technique in the Radball(TM) Technology" *Health Physics,* **102**, 196, (2012).

(8) N. Girault; L. Bosland; S. Dickinson; F. Funke; S. Guentay; L.E. Herranz; D. Powers, "LWR severe accident simulation: Iodine behaviour in FPT2 experiment and advances on containment iodine chemistry" *Nuclear Engineering and Design,* **243**, 371, (2012).

(9) M.T. Harrison; C.J. Steele; A.D. Riley, "The effect on long term aqueous durability of variations in the composition of UK vitrified HLW product" *Glass Technology-European Journal of Glass Science and Technology Part A,* **53**, 211, (2012).

(10) K. Hesketh, "A new non-proliferation assessment tool" *Nuclear Engineering International,* **57**, 36, (2012).

(11) M.R. Mitchell; D. Carnevale; R. Orr; K.R. Whittle; S.E. Ashbrook, "Exploiting the Chemical Shielding Anisotropy to Probe Structure and Disorder in Ceramics: Y-89 MAS NMR and First-Principles Calculations" *Journal of Physical Chemistry C,* **116**, 4273, (2012).

(12) S.A.T. Redfern; S.E. Smith; E.R. Maddrell, "High-temperature breakdown of the synthetic iodine analogue of vanadinite, Pb-5(VO_4)(3)I: an apatite-related compound for iodine radioisotope immobilization?" *Mineralogical Magazine,* **76**, 997, (2012).

(13) S.D. Reilly; A.J. Gaunt; B.L. Scott; G. Modolo; M. Iqbal; W. Verboom; M.J. Sarsfield, "Plutonium(IV) complexation by diglycolamide ligands-coordination chemistry insight into TODGA-based actinide separations" *Chemical Communications,* **48**, 9732, (2012).

(14) M.J. Sarsfield; R.J. Taylor; C. Puxley; H.M. Steele, "Raman spectroscopy of plutonium dioxide and related materials" *Journal of Nuclear Materials,* **427**, 333, (2012).

(15) S.J. Stanley; K. Lennox; E.B. Farfan; J.R. Coleman; J. Adamovics; A. Thomas; M. Oldham, "Locating, quantifying and characterising radiation hazards in contaminated nuclear facilities using a novel passive non-electrical polymer based radiation imaging device" *Journal of Radiological Protection,* **32**, 131, (2012).

(16) P.D. Styman; J.M. Hyde; K. Wilford; A. Morley; G.D.W. Smith, "Precipitation in long term thermally aged high copper, high nickel model RPV steel welds" *Progress in Nuclear Energy,* **57**, 86, (2012).

(17) M. Sypula; A. Wilden; C. Schreinemachers; R. Malmbeck; A. Geist; R. Taylor; G. Modolo, "Use of Polyaminocarboxilic Acids as Hydrophilic Masking Agents for Fission Products in Actinide Partitioning Processess" *Solvent Extraction and Ion Exchange,* **30**, 748, (2012).

(18) S.H. Wallace; S. Shaw; K. Morris; J.S. Small; A.J. Fuller; I.T. Burke, "Effect of groundwater pH and ionic strength on strontium sorption in aquifer sediments: Implications for Sr-90 mobility at contaminated nuclear sites" *Applied Geochemistry,* **27**, 1482, (2012).

(19) G.O.H. Whillock; T.J. Binks; C.J. Donohoe, "Localized Corrosion of Stainless Steel in a Nuclear Waste Cooling Water System-Part 4: Artificial Pit Investigation of Nitrate Inhibition" *Corrosion,* **68**, (2012).

(20) G.O.H. Whillock; T.J. Binks; C.J. Donohoe, "Localized Corrosion of Stainless Steel in a Nuclear Waste Cooling Water System-Part 3: Development of a Large Artificial Pit" *Corrosion,* **68**, 859, (2012).

(21) G.O.H. Whillock; S.E. Worthington; C.J. Donohoe, "Localized Corrosion of Stainless Steel in a Nuclear Waste Cooling Water System-Part 1: Crevice Corrosion Studies" *Corrosion,* **68**, 677, (2012).

(22) R.J. Wilbraham; C. Boxall; R.J. Taylor, "Photocatalytically driven dissolution of macroscopic metal surfaces. Part 1: Silver" *Journal of Photochemistry and Photobiology a-Chemistry,* **249**, 21, (2012).

(23) T.A. York; P.N. Green; P.R. Green; A. Phasouliotis; Z. Qu; S. Watson; M. Hussain; S. Nawaz; N. Trigoni; S. Stanley, "Acoustic Sensor Networks for Decommissioning" *Measurement & Control,* **45**, 48, (2012).

RoSPA 20 11
Winner
RESEARCH & DEVELOPMENT
Sector Award

Winner 2004 - 2008, 2010 - 2011
Highly Commended 2009, 2012, 2013

5th Floor
Chadwick House
Warrington Road
Birchwood Park
Warrington
WA3 6AE

T. +44 (0) 1925 289800
E. customers@nnl.co.uk

W. www.nnl.co.uk

@UKNNL

NATIONAL NUCLEAR LABORATORY